Published in final edited form as:
Geochim Cosmochim Acta. 2016 March 1; 176: 295–315. doi:10.1016/j.gca.2015.10.036.

Accretion timescales and style of asteroidal differentiation in an ^{26}Al-poor protoplanetary disk

K.K. Larsen[*], **M. Schiller**, and **M. Bizzarro**
Centre for Star and Planet Formation, Natural History Museum of Denmark, University of Copenhagen, Øster Voldgade 5-7, DK-1350, Denmark

Abstract

The decay of radioactive ^{26}Al to ^{26}Mg (half-life of 730,000 years) is postulated to have been the main energy source promoting asteroidal melting and differentiation in the nascent solar system. High-resolution chronological information provided by the ^{26}Al–^{26}Mg decay system is, therefore, intrinsically linked to the thermal evolution of early-formed planetesimals. In this paper, we explore the timing and style of asteroidal differentiation by combining high-precision Mg isotope measurements of meteorites with thermal evolution models for planetesimals. In detail, we report Mg isotope data for a suite of olivine-rich [Al/Mg ~ 0] achondritic meteorites, as well as a few chondrites. Main Group, pyroxene and the Zinder pallasites as well as the lodranite all record deficits in the mass-independent component of μ^{26}Mg (μ^{26}Mg*) relative to chondrites and Earth. This isotope signal is expected for the retarded ingrowth of radiogenic ^{26}Mg* in olivine-rich residues produced through partial silicate melting during ^{26}Al decay and consistent with their marginally heavy Mg isotope composition relative to ordinary chondrites, which may reflect the early extraction of isotopically light partial melts from the source rock. We propose that their parent planetesimals started forming within ~250,000 years of solar system formation from a hot (>~500 K) inner protoplanetary disk region characterized by a reduced initial $(^{26}Al/^{27}Al)_0$ abundance (~$1–2 \times 10^{-5}$) relative to the $(^{26}Al/^{27}Al)_0$ value in CAIs of 5.25×10^{-5}. This effectively reduced the total heat production and allowed for the preservation of solid residues produced through progressive silicate melting with depth within the planetesimals. These ‘non-carbonaceous’ planetesimals acquired their mass throughout an extended period (>3 Myr) of continuous accretion, thereby generating onion-shell structures of incompletely differentiated zones, consisting of olivine-rich residues, overlaid by metachondrites and undifferentiated chondritic crusts. In contrast, individual olivine crystals from Eagle Station pallasites record variable μ^{26}Mg* excesses, suggesting that these crystals captured the ^{26}Mg* evolution of a magmatic reservoir controlled by fractional crystallization processes during the lifespan of ^{26}Al. Similar to previous suggestions based on isotopic evidence, we suggest that Eagle Station pallasites formed from precursor material similar in composition to carbonaceous chondrites from a cool outer protoplanetary disk region characterized by $(^{26}Al/^{27}Al)_0 \geq 2.7 \times 10^{-5}$. Protracted planetesimal accretion timescales at large orbital distances, with onset of accretion 0.3–1 Myr post-CAIs, may have resulted in significant radiative heat loss and thus efficient early interior cooling of slowly accreting ‘carbonaceous’ planetesimals.

[*]Corresponding author. kirstenl@snm.ku.dk (K.K. Larsen).

Europe PMC Funders Author Manuscripts

Europe PMC Funders Author Manuscripts

1 Introduction

Mixing and reprocessing of primitive material are important processes during the first few million years lifetime of protoplanetary disks that can affect the composition of resulting planetary bodies. In a protoplanetary disk, the accumulation of dust and ice into planetesimals, and the subsequent differentiation of at least some of these into core, mantle and crust, represents the first critical evolutionary stages towards formation of planetary embryos and ultimately a planetary system. Evidence for the mode and timing of planetesimal melting and differentiation in our solar system is preserved in meteoritic fragments originating from differentiated asteroids. These meteorites preserve evidence of magmatic activity on their parent bodies and, thus, provide 'time-capsules' into the very earliest stages of planetary formation. The signatures of the past decay of radioactive isotopes that were present in our nascent solar system and preserved in ancient meteorites provide powerful chronometers to unravel the timescales of planetesimal accretion and melting. Radiometric ^{182}W deficit dating on iron meteorites, originating from various parent bodies, suggests that large differentiated planetesimals segregated metallic cores within ~1 Myr of formation of the first solar system solids, Ca–Al-rich inclusions (CAIs), suggesting accretion of their parent bodies within the first 300,000 years (Kruijer et al., 2014). Very early onset of planetesimal formation and rapid run-away growth of planetary embryos also seems required from ^{60}Fe–^{60}Ni and ^{182}Hf–^{182}W chronometry on Martian meteorites suggesting that about half the present day size of Mars accreted within 2 Myr of solar system formation (Dauphas and Pourmand, 2011; Tang and Dauphas, 2014). Early formation of basaltic angrite meteorites marks the onset of large-scale volcanic activity on asteroidal surfaces ~3 Myr after formation of CAIs (Amelin, 2008; Connelly et al., 2008; Larsen et al., 2011; Kleine et al., 2012). This meteoritic evidence is also consistent with numerical and analytical models suggesting that formation of large planetesimals and planetary embryos can be a very rapid and efficient process, both in purely laminar disks and in the presence of weak turbulence (e.g. Johansen et al., 2007; Weidenschilling, 2008). Such models indicate that large km-sized bodies may accrete on the order of 10^4–10^5 years at ~1 AU (e.g. Weidenschilling, 2000; Chambers, 2006).

Radioactive ^{26}Al [$t_{1/2}$ = 0.73 Myr] was the primary heat source for early planetesimal melting and differentiation given the large amount of energy released by its decay (e.g. Ghosh et al., 2006; McCoy et al., 2006). The presence of ^{26}Al in the solar system's oldest solids (e.g. Lee et al., 1976; MacPherson et al., 1995; Bizzarro et al., 2004) fuelled the initial stages of planetary differentiation (e.g. Ghosh and McSween, 1998; Bizzarro et al., 2005). The initial abundance of ^{26}Al present at the time of planetesimal accretion, therefore, determines the thermal evolution and ultimate compositional structure of asteroidal bodies. However, accretion of large iron meteorite parent bodies within the first few hundred thousand years of CAI-formation (with ^{26}Al/^{27}Al > ~2 × 10^{-5} assuming ^{26}Al homogeneity with a canonical (^{26}Al/^{27}Al)$_0$ of 5.25 × 10^{-5} defined by CV CAIs; Jacobsen et al., 2008; Larsen et al., 2011) would result in large-scale global melting (e.g. Hevey and Sanders, 2006; McCoy et al., 2006; Sahijpal et al., 2007). Preservation of partial melting residues within asteroidal bodies in the form of primitive achondritic meteorites, such as acapulcoites and lodranites, constitute direct evidence for incomplete melting of planetesimals. Also, the

preservation of undifferentiated chondritic meteorites has been the main reasoning for suggesting delayed onset of accretion of partially differentiated primitive achondrite parent bodies and undifferentiated chondritic parent bodies, i.e. >1.5 Myr after CAIs (e.g. Trieloff et al., 2003; Kleine et al., 2008; Touboul et al., 2009; Henke et al., 2013). Such delayed onset of accretion is in contrast to the very early accretion timescales inferred for iron meteorites (Kruijer et al., 2014). Members of each meteorite group (primitive achondrites, ordinary chondrites and some iron meteorites) are believed to have accreted from the inner solar protoplanetary disk. As such, the current meteoritical view of planetesimal formation within the solar protoplanetary disk involves a time-gap between the onset of formation of large differentiated asteroids and those of undifferentiated chondritic meteorites, such as ordinary chondrites.

However, such disparity in the cosmochemical constraints on planetesimal formation can be reconciled by a reduced initial abundance of ^{26}Al in the accretion regions of large differentiated planetesimals relative to the canonical initial $(^{26}Al/^{27}Al)_0$ value of 5×10^{-5} in CAIs, thereby reducing the extent of asteroid internal heating. For example, based on $^{26}Mg^*$ variability in reservoirs with solar or near-solar Al/Mg ratio, Larsen et al. (2011) proposed that the initial $(^{26}Al/^{27}Al)_0$ in the protoplanetary disk ranged from 1 to 2.8×10^{-5}. Similarly, a recent comparison of U-corrected Pb–Pb and ^{26}Al–^{26}Mg ages of three volcanic angrites indicates that the initial $(^{26}Al/^{27}Al)_0$ of the primitive disk material which accreted to form the angrite parent body was only 1.3×10^{-5} (Schiller et al., 2015a). A reduced initial abundance of ^{26}Al in the protoplanetary disk shortens the timescales for accretion of meteorite parent bodies and brings the thermal constraints from ^{26}Al heating in asteroids in agreement with dynamical models for efficient and rapid planetesimal formation. Therefore, a robust reevaluation of the role of ^{26}Al for asteroidal melting and differentiation, including their accretion timescales and extent of internal differentiation, is required.

The timing of planetesimal accretion and differentiation may be evaluated through the Mg isotope composition of magmatic products of differentiated asteroids. Early formed meteoritic materials that are virtually free of Al and rich in Mg (i.e. with significantly sub-chondritic Al/Mg ratios) are not influenced by the in situ decay of ^{26}Al after their formation and as such preserve the radiogenic ^{26}Mg isotope component of their source reservoir at the time of their formation. In an evolving magmatic system during the lifespan of ^{26}Al, forming olivine (Al/Mg ~ 0) records the Mg isotope composition of the source reservoir (e.g. Schiller et al., 2011; Baker et al., 2012). Pallasite meteorites are high temperature igneous products from the interior of large differentiated asteroids. They consist predominantly of large (mm–cm) forsteritic olivine crystals embedded in metallic Fe–Ni (e.g. Buseck, 1977; Scott, 1977; Haack and McCoy, 2007; Boesenberg et al., 2012) and are therefore ideally suited to track the timing and nature of asteroid differentiation. As such, pallasites that originated from different parent bodies in the inner and outer protoplanetary disk, as indicated by their contrasting O-isotope and $\varepsilon^{54}Cr$ compositions (Clayton and Mayeda, 1996; Shukolyukov and Lugmair, 2006; Trinquier et al., 2007; Warren, 2011), may contain distinct igneous fingerprints of silicate differentiation. Hence, by linking the thermal constraints given by their igneous history through ^{26}Al heating to the chronological information provided by their Mg isotope compositions we can evaluate the ^{26}Al variability in the solar protoplanetary disk.

Considering that a reservoir with solar abundances of Al and Mg containing the maximum $^{26}Al/^{27}Al$ abundance of 5.25×10^{-5} will only increase the $^{26}Mg/^{24}Mg$ ratio by 38 ppm (ppm), precise time constraints for Al-poor extraterrestrial material require very high-resolution data to resolve differences in $\mu^{26}Mg^*$. Taking advantage of novel methods for high-precision Multi-Collector Inductively-Coupled-Plasma Mass-Spectrometry (MC-ICP-MS) and improved chromatographic protocols for magnesium purification (Bizzarro et al., 2011), we report Mg isotope data for a suite of pallasites, including Main Group Pallasites, pallasites from the Eagle Station grouplet, pyroxene pallasites and two un-grouped pallasites, as well as one primitive achondrite, a lodranite meteorite. We use these data to constrain the degree of Mg isotope variability in the solar protoplanetary disk and evaluate the timescales for accretion and differentiation of large differentiated parent bodies. We further examine the influence of potential initial $(^{26}Al/^{27}Al)_0$ variability in the accretion disk on heating timescales and extent of asteroid differentiation using thermal modeling. Finally, we present a novel view of planetesimal formation in the early solar system from a meteorite perspective in which the timescales for accretion and melting of large partially differentiated meteorite parent bodies inferred from their $^{26}Al–^{26}Mg$ isotope systematics are integrated with their thermal evolution.

2 Materials, Methods and Analytical Procedures

2.1 Sampling procedures, chromatographic purification and isotope analysis

Olivine grains from interior parts of 10 Main Group Pallasites (Springwater, Philips County, Dora, Fukang, Brahin, Brenham, Molong, Giroux, Krasnojarsk, Admire), two pyroxene pallasites (Vermillion and Yamato 8451), two pallasites from the Eagle Station grouplet (Eagle Station and Cold Bay) and two ungrouped pallasites (Zinder and Milton) were sampled using either computer-assisted micro-drilling (New Wave Research MicroMill at the Centre for Star and Planet Formation, University of Copenhagen) with tungsten carbide drill bits or by grain picking under binocular microscope. Samples were subsequently transferred to pre-cleaned Savillex PFA beakers in preparation for ion chromatographic purification of Mg. A total of 24 grain fragments from three different specimens of the Eagle Station pallasite were measured for their Mg isotope compositions; 21 grains from a specimen at the Centre for Star and Planet Formation at the University of Copenhagen, one grain from a specimen in the meteorite collection at the Smithsonian Institution, National Museum of Natural History (sample ES-USNM2753) and two grains from a specimen in the meteorite collection at the Geological Museum, Natural History Museum of Denmark (ES-NHMD1890.419a and ES-NHMD1890.419b). Individual olivine grain fragments were sampled from the 15 other pallasite meteorites. A fresh fragment of the lodranite meteorite, NWA 4478, was extracted and crushed to a fine powder with an agate pestle and mortar. A sample (~200 mg) of homogenized sawdust powders (several 10’s of grams) collected from a diamond cutting process of several slabs of the Allende CV3 meteorite, as well as powdered bulk samples of the Murchison CM2 (~200 mg), NWA 6043 CR2 (~200 mg) and NWA 4425 CK3 (~100 mg) chondrites were also sampled for bulk Mg isotope measurements. To remove potential surficial contamination, individual olivine grain fragments (1−3 mm in diameter) were etched in cold, double-distilled dilute HCl in an ultrasonic bath for about 20 min. Samples were digested in Savillex PFA beakers on a

hotplate at 120 °C in mixtures of concentrated HF with a few drops of concentrated HNO_3, evaporated to dryness and re-dissolved in aqua regia (HNO_3:HCl = 1:3). All samples were finally converted to Cl-form and re-dissolved in 6 M HCl in preparation for chromatographic purification of Mg.

Prior to isotopic analysis, Mg was extracted and purified from sample matrices by ion chromatographic separation and Mg-isotope measurements were performed on a Thermo Finnigan Neptune Plus MC-ICPMS located at the Centre for Star and Planet Formation, Natural History Museum of Denmark, University of Copenhagen, according to methods and analytical protocols described in Bizzarro et al., 2011. In brief, Mg was separated using a six step chromatographic purification protocol which combines cation (AG50W-X8 200–400 mesh), anion (AG1-X8 200–400 mesh and TODGA) and Ni-specific resins to efficiently separate Fe, Cr, Al, Ti, V, Ca, Ni, Na, and Mn from the purified Mg aliquot. After SiF_4 volatilization (and thus removal of Si) through the HF-HNO_3 digestion step, the only other major element (other than Mg) present in these olivine-rich samples is Fe. This element is effectively removed in the first chromatographic step by utilizing an anion exchanger exposed to 6 M HCl. Total Mg procedural blanks were less than 10 ng and negligible compared to the typical amount of Mg (~100 μg) analyzed in this study.

Following Mg purification, samples were converted to nitrate form, dissolved in a 2% HNO_3 solution and aspirated into the plasma source by means of the ThermoFisher stable introduction system. Measurements were made in medium resolution mode ($M/\Delta M$ ~5000 as defined by the peak edge width from 5% to 95% full peak height). Samples and standards were typically analyzed with a signal intensity of 100 V on mass 24, and ensuring that the signal intensity of the sample and standard were matched to within 2%. Each analysis comprised a total of 630 seconds of baseline measurements and 1667 seconds of data acquisition (100 scans integrated over 16.67 seconds). Samples were bracketed by analyses of the DSM-3 standard (Galy et al., 2003) and systematically analyzed 10 times.

The magnesium isotopic composition is reported as the parts per million (ppm) deviation relative to the isotope composition of the Mg DSM-3 reference standard: $\mu^{i}Mg = [(^{i}Mg/^{24}Mg)_{sample}/(^{i}Mg/^{24}Mg)_{DSM\text{-}3} - 1] \times 10^{6}$, where $i = 25$ or 26. The mass-independent ^{26}Mg component ($\mu^{26}Mg^{*}$) is reported in the same fashion and calculated by internal normalization to $^{25}Mg/^{24}Mg = 0.126896$ ($^{26}Mg/^{24}Mg = 0.139652$) (Bizzarro et al., 2011) on an individual ratio basis using the exponential mass fractionation law. Data reduction of Mg isotopic data was conducted off-line using the freeware software package Iolite, which runs within Igor Pro (Paton et al., 2011). Changes in mass-bias with time were interpolated using a smoothed cubic spline and the mean and standard error of the measured ratios for each analysis was calculated using a 2 SD outliers rejection threshold. These individual analyses of a sample were combined to produce a weighted mean from the propagated uncertainties of individual analyses and reported final uncertainties are 2 SE of the weighted mean. The long-term reproducibility of our measurements, estimated by repeated analysis of Mg standards and natural reference materials, were 20 ppm and 2.5 ppm for the $\mu^{25}Mg$ and $\mu^{26}Mg^{*}$ values, respectively (Bizzarro et al., 2011). The $^{27}Al/^{24}Mg$ ratios were measured on an X-Series ICP-MS at the Centre for Star and Planet Formation, University of Copenhagen, and are accurate to 2%.

Europe PMC Funders Author Manuscripts

2.2 Thermal modeling

The internal heating of early-formed planetesimals is determined by its absolute ^{26}Al heat budget combined with the influence of radiative heat transfer to space dominated by planetesimal size (e.g. McCoy et al., 2006). Thus, to link the chronological constraints provided by ^{26}Al decay within asteroidal bodies with their thermal history, we performed thermal modeling using ^{26}Al as a heat source. We used the analytical solution to the heat conduction partial differential equation for a spherically symmetric planetesimal with uniformly distributed ^{26}Al and uniform composition, according to Carslaw and Jaeger (1959) and Hevey and Sanders (2006):

$$T=T_0+\frac{\kappa A_0}{K\lambda}e^{-\lambda t}\left[\frac{Rsin\left(r\sqrt{\frac{\lambda}{\kappa}}\right)}{rsin\left(R\sqrt{\frac{\lambda}{\kappa}}\right)}-1\right]+\frac{2R^3A_0}{r\pi^3K}\sum_{n=1}^{\infty}\frac{-1^n}{n\left(n^2-\frac{\lambda R^2}{\kappa\pi^2}\right)}sin\left(\frac{n\pi r}{R}\right)e^{-\frac{\kappa n^2\pi^2 t}{R^2}} \quad (1)$$

where t is the time after accretion, R represents the planetesimal radius and r, the distance from the centre. A_0 denotes the power output from ^{26}Al decay in W m^{-3}, calculated by multiplication of the aluminum (containing ^{26}Al) decay energy in J kg^{-1}, with the weight fraction of Al in the solid, the solid density and the fraction of ^{26}Al left at the time of accretion. We used a revised estimate of the amount of energy released per decay of ^{26}Al of 3.12 MeV (Ferguson, 1958; Schramm et al., 1970; Castillo-Rogez et al., 2009). The other constants are as defined in Table 1. The absolute ^{26}Al heat budget is governed by the total Al abundance in the source rock and ^{26}Al abundance at the time of planetesimal accretion. A constant surface temperature of 250 K (Hevey and Sanders, 2006) corresponding to the ambient temperature, T_0, of the disk was assumed for the first set of simulations. We further examine the influence of elevated ambient disk temperatures (250–1000 K) at the onset of planetesimal accretion on the timescales for silicate differentiation. We also evaluate the influence of instantaneous planetesimal accretion versus incremental accretion on the timescales for planetesimal melting and differentiation. For our incremental accretion model, we assume that the radius, R, increases according to a power law of the form $R = t^{1/\alpha}$, where R_{max} is reached after $t_{duration}$ = 3 Myr of accretion, in accordance with the range of chondrule ages in ordinary chondrites (Connelly et al., 2012). Thus, α is equal to $\ln(t_{duration})/\ln(R_{max})$. The modeling results are in good agreement with those of Hevey and Sanders (2006) and Sahijpal et al. (2007).

2.2.1 Modeling the temperature evolution of the Main Group Pallasite parent body—

Metallographic cooling rates for Main Group Pallasites (MGPs) suggest a final parent body radius of at least 100 km (Haack and McCoy, 2007), at which point (i.e. >50 km in radius) heat loss is considered negligible (e.g. Bizzarro et al., 2005; Hevey and Sanders, 2006). The most prominent temperature-controlling variable that remains is thus the total ^{26}Al budget of the source rock at the time of accretion. We therefore assume a MGP parent body radius of 100 km and source rock composition similar to ordinary chondrites (Al = 1.13 wt%; Density, ρ = 3800 kg m^{-3}; H chondrites (Lodders and Fegley, 1998; Hutchison, 2004)), in accordance with geochemical evidence and their similar ε^{54}Cr signature (Trinquier et al., 2007; Boesenberg et al., 2012). In our model, Fe–FeS eutectic

melting occurs at 1270 K (McCoy et al., 2006). We use a silicate solidus temperature of 1350 K, marking the onset of silicate melting for an ordinary chondrite type of source rock (McCoy et al., 2006). The high degrees of partial melting (i.e. of >50%) required to explain the olivine-only silicate assemblage of pallasite meteorites (e.g. McCoy et al., 2006) constrains the lower bound on the peak temperature experienced by MGP olivine to ~1650 K for an ordinary chondrite type of source rock (Mare et al., 2014). Liquidus temperatures of their forsteritic olivine compositions (Fo = 80–90%) are in the range of 1900–2100 K (Hess, 1989); here we adopt the upper bound of 2100 K.

2.2.2 Modeling the temperature evolution of the Eagle Station parent body—

For the Eagle Station parent body, we assume a planetesimal radius of 100 km, consistent with metallographic cooling rates for the Eagle Station Pallasite (ESP) (Haack and McCoy, 2007; Yang et al., 2010). We use a precursor composition similar to CV carbonaceous chondrites (Al = 1.75 wt%; Density, $\rho = 3420$ kg m^{-3}; Lodders and Fegley, 1998; Hutchison, 2004), in agreement with geochemical evidence and the similar ε^{54}Cr and Δ^{17}O signatures of Eagle Station and CV chondrites (Clayton and Mayeda, 1996; Wasson and Choi, 2003; Shukolyukov and Lugmair, 2006; Trinquier et al., 2007).

3 Results

The mass-dependent magnesium isotope compositions (μ^{25}Mg) of pallasite olivine measured in this study are summarized in Tables 2 and 3 and reported graphically in Fig. 1. The Main Group Pallasites define a mean μ^{25}Mg value of −109 ± 31 ppm (2sd, $n = 10$), which is identical to the Mg isotope composition of bulk silicate Earth (BSE) defined by samples of Earth's mantle (e.g. Handler et al., 2009; Young et al., 2009; Bourdon et al., 2010; Schiller et al., 2010; Teng et al., 2010; Huang et al., 2011; Liu et al., 2011; Pogge von Strandmann et al., 2011; Bizzarro et al., 2011), as well as enstatite chondrites (Larsen et al., 2011). Moreover, the mass-dependent Mg isotope composition of Main Group Pallasites is indistinguishable from that of the two pyroxene pallasites (−120 ± 34 ppm) as well as the ungrouped Milton (−97 ± 20 ppm) and Zinder (−131 ± 20 ppm) pallasites. In contrast, samples from the Eagle Station grouplet record μ^{25}Mg values that are systematically lighter than all other pallasites and BSE, as well as CI chondrites reported in Larsen et al. (2011). It is, however, identical to both our measurement of CK (−178 ± 20 ppm), CV (−169 ± 20 ppm) and CM (−159 ± 20 ppm) carbonaceous chondrites, as well as ordinary chondrites (−171 ± 24 ppm; Larsen et al., 2011). In detail, the population of individual olivine grains from the Eagle Station pallasite as well as an olivine sample from the Cold Bay (Eagle Station group) pallasite define μ^{25}Mg values of −183 ± 23 ppm and −187 ± 20 ppm, respectively, which is 74 ± 38 ppm lighter than that of MGPs. The population of individual grains from the Eagle Station pallasite shows no resolvable μ^{25}Mg variability outside the external reproducibility of 20 ppm for the μ^{25}Mg value using our method (Bizzarro et al., 2011).

The mass-independent component of μ^{26}Mg (μ^{26}Mg*) varies considerably amongst the different pallasite groupings (Fig. 2). Main Group Pallasites show limited variability in μ^{26}Mg*, ranging from −15.0 ± 2.5 ppm to −8.2 ± 2.5 ppm and defining a weighted mean of −10.9 ± 5.0 ppm (2sd). The two pyroxene pallasites, Vermillion and Yamato 8451, have

$\mu^{26}Mg^*$ values of −11.6 ± 2.5 ppm and −14.6 ± 2.5 ppm, respectively, and the ungrouped Zinder has a value of −11.5 ± 2.5 ppm. All these compositions are indistinguishable from that of MGPs. In contrast, the ungrouped Milton defines a $\mu^{26}Mg^*$ of +1.6 ± 2.5 ppm, irresolvable from that of Earth's mantle. Moreover, samples from the Eagle Station grouplet record positive $\mu^{26}Mg^*$ values relative to Earth's mantle. In detail, a single olivine from Cold Bay has a $\mu^{26}Mg^*$ excess of +5.2 ± 2.5 ppm, while individual Eagle Station olivine grains record $\mu^{26}Mg^*$ values ranging from +1.3 ± 1.5 ppm to +14.8 ± 2.0 ppm. The range of 13.5 ppm defined by the population of olivine grains from Eagle Station is well outside the external reproducibility of 2.5 ppm for the $\mu^{26}Mg^*$ value using our approach (Bizzarro et al., 2011). All samples with excess $\mu^{26}Mg^*$ for which the Cr isotope composition has previously been reported (Eagle Station pallasite, CV, CK and CI chondrites) also exhibit excesses in $\varepsilon^{54}Cr$ (Shukolyukov and Lugmair, 2006; Trinquier et al., 2007). Similarly, samples with deficit $\mu^{26}Mg^*$ (MGPs and ordinary chondrites) also exhibit deficits in $\varepsilon^{54}Cr$ (Trinquier et al., 2007).

4 Discussion

4.1 Distribution of ^{26}Al in the solar protoplanetary disk

A chronological interpretation for the observed $\mu^{26}Mg^*$ variability requires knowledge of the initial abundance and distribution of ^{26}Al in the solar protoplanetary disk at the time of solar system formation. It is commonly assumed that the ^{26}Al nuclide was homogeneously distributed amongst solar system solids during the evolution of the solar protoplanetary disk. In this model, the initial canonical $^{26}Al/^{27}Al$ ratio of ~5×10^{-5} (i.e. MacPherson et al., 1995) recorded by the oldest disk solids, calcium-aluminum-rich inclusions (CAIs), is believed to represent the initial abundance of ^{26}Al for the solar system as a whole. This simplistic view, however, has been recently challenged by a number of studies. For example, Larsen et al. (2011) reported heterogeneity in the $\mu^{26}Mg^*$ values of bulk solar system reservoirs with solar or near-solar Al/Mg ratios interpreted as reflecting variability in the initial abundance of ^{26}Al, perhaps up to 80% of the canonical value. Variability in the initial abundance of ^{26}Al is inferred to be correlated with that of nuclides that track nucleosynthetic heterogeneity in disk solids such as ^{54}Cr, ^{48}Ca and ^{50}Ti. This variability is interpreted as reflecting progressive thermal processing of in-falling ^{26}Al-rich molecular cloud material, which resulted in preferential loss by sublimation of thermally unstable and isotopically anomalous presolar carriers, producing residual isotopic heterogeneity. This model, described in detail in previous work (Trinquier et al., 2009; Larsen et al., 2011; Paton et al., 2013; Schiller et al., 2015b), builds on secondary unmixing of dust generations with distinct thermal properties from an initially physically well-mixed disk. Thus, this model is consistent with the idea that stellar-derived dust is efficiently admixed and homogenized in molecular cloud structures. In summary, ^{26}Al and ^{54}Cr-rich presolar silicate carriers are progressively thermally processed during infall of envelope material to the inner protoplanetary disk. As the freshly-synthesised supernova-derived carriers are expected to be more thermally labile compared to older, galactically-inherited interstellar dust, the carriers of ^{26}Al and ^{54}Cr are preferentially incorporated into a gas phase. This results in an enrichment in the abundance of ^{26}Al and ^{54}Cr in the gas phase relative to residual midplane dust, which translates into a positively correlated relationship between $\mu^{26}Mg^*$ and $\mu^{54}Cr$

described by Larsen et al. (2011). Thus, reservoirs characterized by super-solar initial $(^{26}Al/^{27}Al)_0$ ratios record excesses in ^{54}Cr whereas reservoirs typified by sub-solar initial $(^{26}Al/^{27}Al)_0$ ratios record ^{54}Cr deficits.

Although this interpretation of $\mu^{26}Mg^*$ variability in bulk solar system reservoirs with solar or near solar $^{27}Al/^{24}Mg$ ratios has been questioned by some (i.e. Wasserburg et al., 2012), a recent high-resolution comparison of U-corrected Pb–Pb and ^{26}Al–^{26}Mg ages for three angrite meteorites supports the model of initial disk ^{26}Al heterogeneity. Indeed, Schiller et al. (2015a) showed that ^{26}Al–^{26}Mg ages for three rapidly-cooled angrites are systematically younger by ~1.5 Myr relative to their assumption free absolute ages, requiring that the ^{54}Cr-poor angrite parent body formed from material with an initial $(^{26}Al/^{27}Al)_0$ of $1.33^{+0.21}_{-0.18} \times 10^{-5}$. This estimate is identical to that inferred from the $\mu^{26}Mg^*$ value of young angrites ($[^{26}Al/^{27}Al]_0 = 1.61(\pm 0.32) \times 10^{-5}$; Larsen et al., 2011), confirming that most of the $\mu^{26}Mg^*$ variability in bulk solar system reservoirs with solar or near solar $^{27}Al/^{24}Mg$ ratios reflect ^{26}Al heterogeneity (Fig. 3). Given that the meteorites selected here for Mg isotope measurements are derived from parent asteroids with both excesses and deficits in ^{54}Cr relative to Earth, we explore the consequence of a reduced initial ^{26}Al disk inventory relative to the canonical $^{26}Al/^{27}Al$ value for the thermal evolution and timing of accretion of differentiated asteroids.

4.2 Comparison with previous studies

Stable Mg isotope data of pallasite olivines have been reported in a number of earlier studies, including Handler et al. (2009), Young et al. (2009), Chakrabarti and Jacobsen (2010), Villeneuve et al. (2011), Baker et al. (2012) and Luu et al. (2014). Our average $\mu^{25}Mg$ value of −109 ± 31 (2sd) ppm for MGPs compares favorably with the values of −138 ± 47 (2sd) ppm and −116 ± 89 ppm reported by Handler et al. (2009) and Baker et al. (2012), respectively. Similarly, our average $\mu^{25}Mg$ value of −183 ± 23 ppm (2sd) for the 21 individual Eagle Station olivine grains is within uncertainty of the value of −174 ± 48 (2sd) reported for this meteorite using MC-ICPMS by Luu et al. (2014). However, our results are not consistent with the $\mu^{25}Mg$ values reported for Eagle Station and MGPs by Chakrabarti and Jacobsen (2010), which suggest Mg isotope compositions lighter by ~100 ppm relative to our data. Moreover, Villeneuve et al. (2011) reports a $\mu^{25}Mg$ value of ~1300 ppm for the Eagle Station pallasite, which is clearly different from our data as well as that reported by earlier studies. As shown in Luu et al. (2014), the discrepancy in the $\mu^{25}Mg$ value reported by Villeneuve et al. (2011) relative to other studies probably reflects matrix effects. However, the exact nature of the systematic offset observed in the dataset of Chakrabarti and Jacobsen (2010) is unclear at this stage.

High-precision $\mu^{26}Mg^*$ data with an external reproducibility comparable to that obtained in our study has only been published by Baker et al. (2012) who reported $\mu^{26}Mg^*$ values for Main Group Pallasites ranging from −9.6 ± 4.3 to −13.1 ± 3.0, which is in excellent agreement with our data. Using secondary ionization mass spectrometry (SIMS), Villeneuve et al. (2011) reported on the in situ Mg isotope systematics of individual olivine grains from the Eagle Station pallasite. In contrast to our data, their measurements show systematic deficits in the $\mu^{26}Mg^*$ of −33 ± 8 ppm (2sd = 44 ppm), which the authors attribute to

differentiation of the Eagle Station parent body coevally with the condensation of CAIs. However, these results are not consistent with our high-precision data for the same meteorite and, similarly to other authors (Baker et al., 2012; Luu et al., 2014), we suggest that the systematic $\mu^{26}Mg^*$ deficits reported by Villeneuve et al. (2011) reflect an analytical artifact. More recently, Luu et al. (2014) reported $\mu^{26}Mg^*$ data for the Eagle Station pallasite using both MC-ICPMS and SIMS techniques, although the uncertainties of these measurements for individual samples vary from about 10 to 30 ppm. Using a mass-fractionation factor, β, of 0.521 for mass-bias correction, these authors define an average $\mu^{26}Mg^*$ value of 0 ± 6 ppm (2sd = 48 ppm) for their MC-ICPMS data. Re-calculating $\mu^{26}Mg^*$ values reported in Luu et al., 2014 using the exponential law ($\beta = 0.511$; this study), elevates the average $\mu^{26}Mg^*$ to about +7 ppm due to residual mass-fractionation effects, i.e. within range of reported $\mu^{26}Mg^*$ for Eagle Station olivines in this study. Similar to Villeneuve et al. (2011), the SIMS data reported by Luu et al. (2014) show systematic deficits in $\mu^{26}Mg^*$ (also when re-calculated using the exponential law), defining an average value of −11 ± 9 ppm (2sd = 44 ppm) and, thus, inconsistent with our result. Evidently, the results of Villeneuve et al. (2011) and Luu et al. (2014) demonstrate the challenges of using SIMS instruments to obtain high-precision and accurate Mg isotope measurements of single minerals.

4.3 Origin of the mass-dependent Mg isotope variability

4.3.1 Mass-dependent Mg isotope heterogeneity of the precursor material?—

Nebular processes could have resulted in spatial or temporal isotope variability through evaporation, condensation, mixing or unmixing of primitive disk solids. Indeed, various meteorite groups exhibit highly contrasting $\varepsilon^{54}Cr$, $\varepsilon^{50}Ti$ and oxygen isotopic compositions, indicative of their differing accretion regions within the protoplanetary disk (Warren, 2011). Yet, the relatively small $\mu^{25}Mg$ variability, i.e. <40 ppm, observed between ordinary and carbonaceous chondrites (Fig. 1) with up to ~200 ppm and ~500 ppm difference in $\varepsilon^{54}Cr$ and $\varepsilon^{50}Ti$ (Trinquier et al., 2007, 2009), respectively, indicates that the primitive precursor material across the accretion disk was relatively homogeneous in Mg isotopes. Based on their distinctive mass-independent excesses in $\varepsilon^{54}Cr$ and $\varepsilon^{50}Ti$ (Trinquier et al., 2007, 2009; Warren, 2011) and spectral affinities to C-, P- and D-type asteroids (which dominate the outer asteroid main belt; semimajor axis > 2.8 AU; Gradie and Tedesco, 1982; Asphaug, 2009), carbonaceous chondrites and a few anomalous achondrites, including Eagle Station Pallasites (collectively termed carbonaceous planetesimals), have been proposed to have accreted in the cooler outer regions of the protoplanetary disk (Warren, 2011). According to this model, the outer disk regions were chemically and isotopically fundamentally distinct from the inner accretion regions of non-carbonaceous (e.g. ordinary) chondrites and most achondritic meteorites, including Main Group Pallasites (collectively termed non-carbonaceous planetesimals), characterized by deficits in $\varepsilon^{54}Cr$ and $\varepsilon^{50}Ti$ (Trinquier et al., 2007, 2009; Warren, 2011) and spectral albedo similar to S-, E- and M-type asteroids (which dominate the inner asteroid main belt; semimajor axis <2.8 AU; Gradie and Tedesco, 1982; Asphaug, 2009; Nakamura et al., 2011). This evidence for compositional diversity amongst asteroids in the main belt with radial distance from the Sun was originally attributed to a remnant thermal gradient across the limited heliocentric distances covered by main belt asteroids from ~2 to 3.3 AU (Gradie and Tedesco, 1982). This view has recently changed towards much more dynamical settings in which the compositional gradients were generated

through substantial scattering and partial mixing of early-formed planetesimals originating from inner and outer regions of the solar protoplanetary disk, plausibly related to the early gas-driven migration of the Jovian planets, known as the Grand-Tack model, which was originally proposed to explain the low mass of Mars (Walsh et al., 2011; DeMeo and Carry, 2014). Specifically, Walsh et al. (2011) proposed that S-type asteroids from the inner main belt originally formed within 3 AU from the proto-Sun, whereas C-type asteroids originated between the Jovian planets and beyond, i.e. semimajor axis >~4 AU. In this view, the compositional and isotopic diversity amongst meteorites testifies to large-scale heterogeneities across the accretion disk at the onset of planetesimal formation.

In detail, the Eagle Station pallasite has ε^{54}Cr and Δ^{17}O similar to carbonaceous CO/CV/CK chondrites at ~0.6−0.9 and ~−5, respectively, suggesting formation from similar precursor material (Clayton and Mayeda, 1996; Shukolyukov and Lugmair, 2006). This is in accordance with the identical μ^{25}Mg of ESPs to CV/CK chondrites measured in this study, although equally identical to the non-carbonaceous ordinary chondrites (OCs) that carry deficits in ε^{54}Cr characteristic of inner solar system materials (Fig. 1). The carbonaceous chondrite affinity of ESPs is also supported by their ~50 times enrichment of the refractory element Iridium in its metal phase relative to Main Group Pallasites (Wasson and Choi, 2003). These observations strongly support formation of its parent body in the outer regions of the protoplanetary disk. In this context, the marginally lighter Mg isotope composition of ESPs relative to solar average dust represented by CI carbonaceous chondrites (Fig. 1) can be explained by variable admixing of isotopically anomalous chondritic components, such as refractory inclusions (Ca–Al-rich inclusions [CAIs] and Amoeboid Olivine Aggregates [AOAs]), to the precursor material of carbonaceous planetesimals. Indeed, carbonaceous chondrites are characterized by relatively high proportions of refractory inclusions, which are virtually absent from non-carbonaceous chondrites, such as ordinary and enstatite chondrites (Krot et al., 2007). The mass-dependent Mg isotope variability amongst chondrules is generally restricted to a few tens to hundreds of parts-per-million (Bizzarro et al., 2004; Bouvier et al., 2013), whereas refractory inclusions commonly exhibit anomalies of several per-mil (e.g. Larsen et al., 2011; MacPherson et al., 2012). The Mg isotope budget of refractory inclusions is further dominated by AOA material rich in Mg-olivine (forsterite) whose condensation origin results in isotopically light Mg (Davis and Richter, 2007); typically μ^{25}Mg = ~−1500 ppm in CV AOAs (Larsen et al., 2011). Therefore, the relatively high proportion of AOAs in a range of carbonaceous chondrites (~5 vol% in CV; Krot et al., 2007) can result in slightly lighter bulk Mg isotope compositions in carbonaceous chondrite type of precursor material by ten’s of ppm and thus may explain the slightly lighter Mg in ESPs relative to CAI/AOA-free CI chondrites.

4.3.2 Stable Mg isotope fractionation during asteroidal differentiation?—

Based on geochemical evidence, Main Group Pallasite olivine, like lodranites and acapulcoites, are believed to have originated as solid residues from partial melting of precursor material similar in composition to ordinary chondrites (Dodd, 1981; Mittlefehldt et al., 1996; Boesenberg et al., 2012). This genetic relationship is also supported by the similar ε^{54}Cr deficit of MGPs and OCs (Trinquier et al., 2007) and suggests formation from the inner protoplanetary disk (Warren, 2011), i.e. isotopically (ε^{54}Cr and ε^{50}Ti) and

chemically distinct from the accretion regions of carbonaceous chondrites (CCs) and the Eagle Station parent body. If correct, the identical μ^{25}Mg of OCs to that of CCs suggests that the inner and outer regions of the accretion disk were relatively homogeneous in Mg isotopes. Hence, although MGPs may sample an unknown and isotopically anomalous type of precursor material, we explore the possibility that the 62 ± 39 ppm heavier Mg isotope composition of MGPs, as well as the lodranite and acapulcoite, relative to OCs (Fig. 1) may have resulted from secondary asteroidal differentiation processes.

Equilibrium isotope fractionation (e.g. associated with magmatic evolution) is known to increase considerably with decreasing temperature (Bigeleisen and Mayer, 1947; Young et al., 2009; Teng et al., 2010; Schauble, 2011) and its influence on the Mg isotope composition of high-temperature (>1200 K) ultramafic and basaltic terrestrial rocks has been found to be within analytical uncertainty, i.e. <~100 ppm/amu (Teng et al., 2010; Bourdon et al., 2010). Thus, the high-temperature (>1650 K) origin of pallasite olivines argues against large mass-dependent isotope fractionation during their formation. It is, however, possible that extraction of an isotopically light lower temperature component from a chondritic source rock fractionated the MGP olivine residue towards a slightly heavier Mg isotope composition. Although, core-mantle differentiation processes can result in mass-dependent isotope fractionations for Fe and Si (Poitrasson et al., 2005; Georg et al., 2007; Fitoussi et al., 2009), the high pressure necessary to partition Mg into metallic iron (Dubrovinskaia et al., 2005; Kádas et al., 2009) is at odds with the much lower pressures attained in asteroid sized bodies, such as those of pallasites. At these low-pressure regimes, on the other hand, equilibrium mass-dependent isotope fractionation through igneous differentiation processes becomes more important because of the lower temperatures required for melting. For example, we speculate that low temperature extraction of isotopically light magnesium sulfide (MgS, Niningerite), which has previously been envisioned as floaters at Earth's core-mantle boundary (Herndon, 1996), toward the core regions of larger differentiated asteroids may shift the bulk Mg isotope composition of the residue. Indeed, theory predicts that inter-mineral Mg isotope fractionation in MgS could be extremely negative relative to common Mg-rich rock-forming minerals (Schauble, 2011). However, mass balance calculations suggest that ~1% of the initial Mg must be extracted in the form of MgS to explain the heavy μ^{25}Mg of MGPs relative to ordinary chondrites, which seems at odds with their known sulfur contents (e.g. ~2 wt% S in H chondrites, out of which most partition into FeS; Lodders and Fegley, 1998).

An alternative explanation is extraction of an isotopically light partial melt from a MGP olivine residue. This is in accordance with thermodynamic predictions for a low coordination environment as well as short/strong metal–ligand bonds favoring a heavy isotope composition (Bigeleisen and Mayer, 1947; Urey, 1947; Schauble, 2004, 2011). Experimental observations further indicate that cations in silicate melts generally have higher coordination numbers than in their corresponding crystals (e.g. Henderson et al., 2006), which in turn decreases the bond strength (Nesse, 2000) and thus favors an isotopically light melt composition. Also, experimental evidence suggests that an excess of network formers, such as Al^{3+}, Fe^{3+} or B^{3+}, in the melt compared to the abundance of chargebalancing cations, such as Mg^{2+}, increases the coordination number of these charge-balancing cations (Kroeker and Stebbins, 2000; Mysen and Richet, 2005) and therefore

should further enhance a light Mg isotope composition of the silicate melt. Collectively, thermodynamic predictions for Mg isotope fractionation combined with experimental observations for bonding environments in silicate melts supports the idea that a low temperature melt extracted from an olivine-rich solid residue should become isotopically light in Mg. Assuming equilibrium partitioning of Mg between silicate melt and source rock during batch melting (White, 2013) of an H-type ordinary chondrite and using the Mg isotope compositions of ordinary chondrites and MGPs, mass balance calculations suggest that at 50% melting the silicate melt should acquire μ^{25}Mg of ~−300 ppm, i.e. 190 ppm/amu lighter than MGPs. Nonequilibrium removal of smaller melt fractions through fractional melting, which may be more likely, would progressively decrease this difference. The partial melt is therefore predicted to record μ^{25}Mg > −300 ppm. Hence, although no direct evidence for such isotopically light partial melts currently exists, we suggest that melt extraction, which evidently occurred within asteroid interiors, may explain the observed MGP heavy Mg isotope composition as compared to an ordinary chondrite type of source rock. If correct, the unfractionated stable Mg isotope composition of Eagle Station olivine relative to its presumed CV/CO/CK-like precursor material (Fig. 1) suggests an intrinsic difference in the magmatic origin of Eagle Station olivine versus MGP olivine, plausibly related to diverse thermal histories of their parent bodies. We further explore this possibility.

4.4 Thermal histories of meteorite parent bodies

In agreement with differences in the μ^{25}Mg between Eagle Station and Main Group Pallasite olivines, μ^{26}Mg* signatures of olivine from both groups further corroborate an inherent difference in their magmatic history. In detail, the relatively homogeneous μ^{26}Mg* deficits observed for MGPs are expected from retarded ingrowth of radiogenic ^{26}Mg in a residue formed by partial melting of a primitive source rock during the lifetime of ^{26}Al (Fig. 4a). Olivine records the Mg isotope composition of the source rock at the time of extraction and partitioning of Al into partial melts. This effectively reduces the Al/Mg ratio to zero in the residue and prevents any further build-up of radiogenic ^{26}Mg* from ^{26}Al decay and thus creates a ‘sub-chondritic’ isotopic time stamp for this event, interpreted to represent the timing of silicate differentiation within the parent body. In agreement with previous Mg isotope data for MGPs (Baker et al., 2012) and geochemical indications for a residue origin (Boesenberg et al., 2012), the ten Main Group Pallasites analyzed here record such predicted limited variability and negative μ^{26}Mg* values suggesting large-scale partial melting during the initial differentiation of their parent body. The similar deficit μ^{26}Mg* of MPG olivine to that recorded by pyroxene pallasites and primitive achondritic meteorites (Fig. 2), whose residue origin is evident from textural and geochemical observations (e.g. Mittlefehldt et al., 1996), further support residue origins for such materials.

Such process cannot easily account for the variable and elevated μ^{26}Mg* of the Eagle Station pallasite olivines. However, these signatures are expected if individual olivines formed through fractional crystallization during the lifetime of ^{26}Al from a common source magma, thereby tracking the composition of this evolving parent magma through time (Fig. 4a; Schiller et al., 2011). If correct, the cumulate olivine records the μ^{26}Mg* of their magmatic source reservoir at the time of crystallization. Inherent to fractional crystallization is also that ongoing crystallization of olivine will continuously increase the Al/Mg ratio of

the source. This generates an ingrowth of $\mu^{26}Mg^*$ in the remaining source reservoir if significant magmatic fractionation occurs while ^{26}Al is still abundant and, as such, can generate elevated $\mu^{26}Mg^*$ as compared to the original bulk source rock. Thus, contrarily to the formation of olivine residues, individual olivines formed by fractional crystallization capture the evolving $\mu^{26}Mg^*$ composition of the parent magma. Hence, the $\mu^{26}Mg^*$ variability recorded for individual olivines within the Eagle Station pallasite is best explained if these olivines formed as cumulates through fractional crystallization during the lifetime of ^{26}Al. Although a cumulate origin seems to be the most likely origin of the ESP olivine, we acknowledge that the mechanism required to subsequently mix individual crystals is not understood.

Although chemically and petrologically similar, the difference in the genesis that we infer for different pallasite olivines revealed by their isotopic composition presents an opportunity to evaluate the thermal history of their individual parent bodies. Formation of Main Group pallasite olivines as solid residues from incomplete melting indicates low sub-liquidus peak temperatures. The apparently efficient metal–silicate separation and the olivine-only silicate assemblage of pallasite meteorites also constrains a lower bound on the degree of partial melting of >50% (e.g. McCoy et al., 2006). Under these conditions, the formation of olivine residues may result in its observed heavy Mg isotope composition created by the extraction of a lower temperature isotopically light basaltic/pyroxenitic partial melt. In contrast, a fractional crystallization origin of Eagle Station olivine requires higher degrees of melting with high peak temperatures. Without significant melt extraction from the source, higher peak temperatures result in isotopic homogenization of the magmatic source reservoir as suggested by the identical $\mu^{25}Mg$ signature of ESPs to their presumed CV/CO/CK-type of chondritic precursors. Retarded melt extraction from a CV-type of protolith is also supported by density differences between the undifferentiated source rock and its extracted chondritic melt, thereby generating relatively large buoyancy contrasts (Fu and Elkins-Tanton, 2014). Through subsequent cooling and high temperature crystallization, cumulate ESP olivines form and record the mass-dependent Mg isotope composition of the source rock as well as radiogenic $\mu^{26}Mg^*$ inherited through magmatic evolution at the time of their crystallization.

4.5 Constraining planetesimal accretion and differentiation timescales in the early solar system

^{26}Al was the dominant heat source for asteroid melting and differentiation in the early solar system (e.g. McCoy et al., 2006). Consequently, the production of radiogenic $\mu^{26}Mg^*$ from ^{26}Al decay, and thus ^{26}Al–^{26}Mg chronology, is intrinsically linked to the thermal evolution of planetesimals that formed within the first few million years of our solar systems formation. Thus, a combined study of $\mu^{26}Mg^*$ evolution and thermal modeling of planetesimal heating is powerful to disentangle the formation timescales of various meteoritic materials. To this effect, we performed thermal modeling of the internal temperature evolution of large km-sized planetesimals heated by the decay of ^{26}Al, including the influence of incremental accretion on radiative heat loss.

4.5.1 Early accretion and melting of partly differentiated planetesimals with onion-shell structures from the inner protoplanetary disk—

If the solar

protoplanetary disk as a whole was characterized by a canonical initial $(^{26}Al/^{27}Al)_0$ of 5.25 × 10^{-5} defined by refractory inclusions in CV chondrites (Jacobsen et al., 2008; Larsen et al., 2011), the $\mu^{26}Mg^*$ deficit recorded by MGP olivine resulting from ^{26}Al decay requires onset of silicate differentiation ~1.5 Myr after CAI-formation, t_0 (Fig. 4b). Combined with our thermal models for differentiation of planetesimals heated by ^{26}Al decay, this implies that the onset of MGP parent body accretion occurred ~1 Myr after CAI-formation (Fig. 5b). On the other hand, the MGP $\mu^{26}Mg^*$ deficit may also be interpreted in the framework of an inner disk accretion region characterized by a reduced initial $(^{26}Al/^{27}Al)_0$ relative to the canonical value (Larsen et al., 2011; Schiller et al., 2015a). We estimate an initial $(^{26}Al/^{27}Al)_0$ in the range of 1−2 × 10^{-5} (Fig. 4b), i.e. similar to previous estimates for the angrite parent body of 1.61(±0.32) ×10^{-5} (Larsen et al., 2011) and $1.33^{+0.21}_{-0.18} \times 10^{-5}$ (Schiller et al., 2015a). At this level, onset of planetesimal accretion must have occurred within 0.5 Myr of CAI-formation in order to achieve 50% melting as recorded by these pallasites (Fig. 5b). The lowest $\mu^{26}Mg^*$ measured for MGP olivines reduces this time interval to < 0.25 Myr post-CAIs (Fig. 4b), in agreement with the predicted onset of angrite parent body accretion within 0.25 Myr of CAI-formation (Schiller et al., 2015a). Fig. 6 shows the chronological significance of a reduced initial $(^{26}Al/^{27}Al)_0$ of 1−2 × 10^{-5} in the accretion regions of large planetesimals that formed within 0.25 Myr of CAI-formation. Back-projecting the corresponding $^{26}Al/^{27}Al$ ratios inferred at the time of accretion of these planetesimals to a 'canonical' initial $(^{26}Al/^{27}Al)_0$ of 5.25 × 10^{-5} results in a delay in their accretion times of 1.25−1.75 Myr post-CAIs.

In accordance with the very early accretion timescales inferred from a reduced $(^{26}Al/^{27}Al)_0$ for noncarbonaceous planetesimals, we note that recent dynamical models for planetesimal formation indicate that planetesimals with sizes up to several hundred kilometers can be accreted very rapidly, indicative of a very short initial accretion history (e.g. Chambers, 2004; Johansen et al., 2007; Cuzzi et al., 2008). This initially efficient planetesimal formation process may have been succeeded by planetesimal disruptions through mutual impacts, thereby resulting in the current size distribution of the asteroid belt in which smaller sub-km objects are predicted to be fragments of once larger planetesimals (Morbidelli et al., 2009). This observation combined with ancient U-corrected Pb–Pb ages of cm-sized chondrules in primitive chondrites, suggests that the initial seeds for planetesimal formation were already present when CAIs formed (Connelly et al., 2012), i.e. at the beginning of solar system formation, thereby providing a pathway to very early accretion of meteorite parent bodies. Such early and rapid planetesimal formation timescales are also consistent with that inferred from ^{182}W deficit dating on magmatic iron meteorites, i.e. accretion < 0.3 Myr after CAIs (Kruijer et al., 2014). Some of these iron meteorites, which once constituted the cores of large differentiated asteroids (Haack and McCoy, 2007), also have similar deficit $\varepsilon^{54}Cr$ to that of MGPs (Trinquier et al., 2007) indicating formation from similar inner disk material. Furthermore, the presence of an ancient core dynamo within the MGP parent body itself is supported by the presence of remnant magnetization in pallasite olivine grains and further supports a genetic relationship between pallasites and iron meteorites (Tarduno et al., 2012), and thus early accretion of their parent bodies. Based on this evidence, we suggest that such early-formed large differentiated planetesimals accreted from an inner ^{26}Al-poor protoplanetary disk, thereby resulting in suppressed heat production

from ^{26}Al decay within their interiors. This early and initially rapid planetesimal accretion stage was most likely followed by continuous accretion throughout the disk lifetime, as exemplified by the 0–3 Myr post-CAI absolute Pb–Pb age spread of chondrules within chondritic meteorites (Connelly et al., 2012). A low ^{26}Al heat production would have resulted in formation of large partly differentiated planetesimals, which may have been a common and widespread process in the inner solar system (Fig. 10).

We further evaluate the typical fate and interior structure of planetesimals accreting from disk material with a reduced initial $(^{26}Al/^{27}Al)_0$. Fig. 7 represents a thermal model showing the temperature evolution as a function of depth within a large planetesimal of ordinary chondritetype of composition, which formed with a $(^{26}Al/^{27}Al)_0$ ratio of 1.6×10^{-5} and continued accreting material throughout 3 Myr of evolution to a final radius of 100 km. This accretion timescale is comparable to the average lifetime of protoplanetary disks around young T-tauri stars (Williams and Cieza, 2011) and the timespan deduced from Pb–Pb ages for chondrules, which signifies that disk material was available for accretion until at least 3 Myr after CAI formation (Connelly et al., 2012). The model shows that the interior peak temperature decreases with distance from the planetesimal centre, thereby resulting in a decrease in the degree of melting experienced by the source rock (Fig. 7). Because of the high melting temperatures of olivine, the final, partly differentiated, onion-shell structure of the planetesimal (Fig. 7, top sketch) consists of an interior part with increasingly olivine-rich silicate residues with increasing depth. This inner zone is overlaid by a thick outer undifferentiated chondritic crust acquired after ~1 Myr post-accretion onset that never experiences peak temperatures in excess of the silicate solidus. This outer, partly metamorphosed crust may be partly overprinted by periodic extrusion of basaltic/pyroxenitic melts originating from greater depths as predicted by the marginal buoyancy contrast resulting from density differences between ordinary chondrite-type of source rocks and their chondritic melts (Fu and Elkins-Tanton, 2014). The downward migration of early-formed, high-density metallic melts results in formation of an Fe-Ni core in the planetesimal centre, which may require at least 50% silicate melting for efficient segregation (McCoy et al., 2006). Such high degrees of partial melting are evident from the olivine-only silicate assemblage of pallasites. The exact depth at which a given melting temperature is reached within the interior of the planetesimal and thus the volume fraction of partial melting residues depends on the details of the accretion process, the extent of melt migration, the influence of convective heat loss and exact ^{26}Al abundance at the time of accretion. Although convective heat loss and melt migration may redistribute interior heating, we note that the shallow thermal gradients required by the final, partly differentiated, onion-shell structure presented in Fig. 7 is best explained if the planetesimal formed with a reduced ^{26}Al abundance relative to the canonical value, interpreted either as delayed accretion > 1 Myr post-CAIs or a sub-canonical initial $(^{26}Al/^{27}Al)_0$ abundance in the accretion disk. Only a very thin fragile chondritic crust is preserved if the planetesimal formed from precursor material with $(^{26}Al/^{27}Al)_0$ of $>\sim 2 \times 10^{-5}$ (Sanders and Scott, 2012). This is because heat redistribution, through convection and melt migration, decreases the thickness and chance of preservation of the undifferentiated chondritic crust with increasing $^{26}Al/^{27}Al$. Heat loss through convection is only efficient at more than 50% melting, thereby resulting in suppressed heating that may prevent complete melting of the interior irrespective of

initial $^{26}Al/^{27}Al$ (Neumann et al., 2014). Similar differentiation scenarios has been presented for carbonaceous chondrite-type of planetesimals in which the partially differentiated interior structure is acquired by onset of accretion > 1 Myr post-CAIs and assuming a canonical initial $(^{26}Al/^{27}Al)_0$ (Sahijpal and Gupta, 2011; Elkins-Tanton et al., 2011).

The $^{182}Hf–^{182}W$ evidence for very early core segregation on large differentiated asteroids (Kruijer et al., 2014) with deficits in $\varepsilon^{54}Cr$ and $\varepsilon^{50}Ti$ (Trinquier et al., 2007) coupled with evidence for paleomagnetization resulting from core dynamo activity within a range of large internally differentiated chondrite parent bodies (H chondrites (Weiss and Elkins-Tanton, 2013), CV chondrites (Carporzen et al., 2011) and R chondrites (Cournède et al., 2014)) is not easily explained by very early planetesimal formation with a canonical $^{26}Al/^{27}Al$ ratio of $\sim 5 \times 10^{-5}$. Planetesimal accretion with such high levels of ^{26}Al would result in global melting of the planetesimal with little chance of survival of thick undifferentiated chondritic crusts (e.g. Hevey and Sanders, 2006). We infer that the occurrence of early-formed (<0.25 Myr after CAIs) partly differentiated planetesimals with onion-shell structures (as presented in Fig. 7), generated through suppressed internal heating from a reduced initial ^{26}Al abundance, may have been the rule rather than the exception in these regions of the protoplanetary disk (Fig. 10). Moreover, the highly variable degrees of thermal metamorphism experienced by ordinary chondrite meteorites (e.g. Scott and Krot, 2007) can be explained by the thermal constraints of our planetesimal formation model if such material accreted to the outer layers of internally differentiated planetesimals that started to form much earlier. According to our model, this material must have accreted onto the growing planetesimal ~1−3 Myr after onset of accretion with the least metamorphosed chondritic material comprising the younger outer crustal regions. The late accretion of ordinary chondrites is also supported by absolute U-corrected Pb–Pb dating of chondrules within un-metamorphosed specimens, spanning a time range up to ~3 Myr post-CAIs (Connelly et al., 2012). This model contrasts to the conventional view of an ordinary chondrite parent body that acquired its metamorphosed onion-shell structure through thermal metamorphism on a late (>~2 Myr) accreting asteroid that never experienced internal peak temperatures in excess of the silicate solidus (Trieloff et al., 2003; Kleine et al., 2008; Henke et al., 2013; Monnereau et al., 2013). Instead, the model permits widespread and late accretion (>1 Myr after CAIs) of chondritic material onto early-formed large internally differentiated planetesimals from the inner solar protoplanetary disk throughout its lifetime and eliminates the need for a time-gap of <2 Myr between the onset of formation of differentiated iron meteorite parent bodies and those of undifferentiated chondrites (e.g. Kleine et al., 2008; Pfalzner et al., 2015).

The final interior structure of such partially differentiated onion-shell planetesimals (Fig. 7) further predicts the preservation of solid residues produced through lower degrees of partial melting than those experienced by MGPs, i.e. <50% melting (McCoy et al., 2006). Such residual rocks would originate at depths intermediate between MGP olivine and the un-differentiated, partly metamorphosed, chondritic crust (Fig. 7) and may be represented by primitive achondritic meteorites such as lodranites and acapulcoites, whose texture and geochemistry indicate partial melting degrees of 5–20% and <5%, respectively (McCoy et al., 1997; Mittlefehldt et al., 1998), as well as pyroxene pallasites which experienced 30–50% melting (McCoy et al., 2006). Interestingly, this decrease in the degree of partial

melting experienced by primitive achondrites and pallasite olivines seems to crudely anti-correlate with their measured $\mu^{26}Mg^*$ values, indicative of increased ingrowth of $^{26}Mg^*$ from ^{26}Al decay in their source rock with decreasing degree of partial melting. This is in agreement with a temporal imprint on the onset of silicate differentiation with depth within their parent bodies, as envisaged in Fig. 7. In detail, the increasing $\mu^{26}Mg^*$ values going from MGPs (−14.9 ± 2.5 to −8.2 ± 2.5 (2sd) ppm; Table 2), pyroxene pallasites (−12.4 ± 2.5 ppm), the lodranite (−9.7 ± 2.5 ppm; Table 2), and to the acapulcoite (−6.0 ± 2.5 ppm; Larsen et al., 2011) and ordinary chondrites (−4.1 ± 2.5 ppm; Larsen et al., 2011), suggests their formation in this order. Although such correlation may be speculative and needs further confirmation, it is in agreement with the predictions of the thermal model where silicate melting begins in the deep interior of the planetesimal and progresses outwards as accretion proceeds (Fig. 7). Deep layers thus experience the highest peak temperatures and thus higher degrees of partial melting (as recorded by MGPs) than regions closer to the surface. An outward migration of peak temperature with time is further supported be the seeming intrusion of lodranitic basaltic melts into overlying acapulcoite rocks (McCoy et al., 1997).

Dynamical disk evolution models show a steep temperature gradient within 1 AU in the first few 10^5 years to over 500 K (Ciesla, 2008; Boss and Ciesla, 2014), suggesting that the ambient disk temperature in these regions of the accretion disk must have been elevated at early times. Thus, such higher disk temperatures must have influenced the interior thermal evolution of planetesimals that started to form within this timeframe. To explore this further, we used the integral relationship between the temperature evolution of planetesimals heated by ^{26}Al decay and the production of radiogenic ^{26}Mg in its source rocks. This allows us to directly link measured $\mu^{26}Mg^*$ values in residual solids with the temperature constraints given by the onset of silicate differentiation and thus melt extraction. This approach suggests that the early onset of silicate differentiation required by the $\mu^{26}Mg^*$ values of MGP olivines is best explained if the ambient temperature of the disk at the time of accretion was higher than 550 K (Fig. 8), i.e. in accordance with disk evolution models.

The proposed continuous accretion model reconciles the very early timescales for onset of core-formation on large differentiated planetesimals (i.e. <0.25 Myr after CAI-formation) with the late formation of undifferentiated chondritic meteorites (>2 Myr) in a coherent planetesimal formation model for the inner accretion disk. In this view, the parent bodies of iron meteorites are the progenitors of subsequent generations of partial melting residues and their magmatic products. In accordance with ancient U-corrected Pb–Pb and Hf–W ages (3–10 Myr) of basaltic meteorites (Amelin, 2008; Connelly et al., 2008; Larsen et al., 2011; Kleine et al., 2012), the model further predicts partial melt extraction and preservation of early-formed basaltic rocks that intruded into or erupted onto the cooler outer layers within the first few Myr of solar system formation. Also, in accordance with the ancient U-corrected Pb–Pb age of the basaltic achondrite Asuka 881394 of 4565.57 ± 0.55 Myr (i.e. ~1.7 Myr post-CAIs; Koefoed et al., 2015), our model allows for silicate differentiation and thus formation of basaltic melts already from an age of ~0.5 Myr after CAIs (Fig. 8). The extraction of such melts from the planetesimal interior and outward migration to cooler regions where they can solidify may require several 100’s of kyr depending on the viscosity of the melt (Moskovitz and Gaidos, 2011). We further note that, in agreement with our results and interpretations, recent numerical simulations suggest that the main growth phase

of asteroids greater than 200 km in diameter occurs via continuous gas-drag-assisted accretion of chondrules over timescales of ~3 Myr (Johansen et al., 2015). Thus, continuous accretion seems to be an unavoidable outcome of the planetesimal formation process. We note, however, that our model has no direct implication for the physical mechanism behind the subsequent mixing of olivine and metal, which make up the final pallasite mineral assemblage. Given that the olivine was solid when molten metal was injected, this mixing event must post-date the formation of the olivine (Scott, 1977) and as such may either have occurred at the core-mantle boundary of the parent body (e.g. Wasson and Choi, 2003) or by subsequent exterior metal mixing through impact processes (e.g. Tarduno et al., 2012). The olivine and metal components, however, almost certainly formed relatively deep within differentiated planetesimals.

4.5.2 Protracted formation timescales for planetesimals in the outer protoplanetary disk—

In contrast to Main Group and pyroxene pallasites, the affinity of the Eagle Station pallasites to CV/CO/CK carbonaceous chondrites in terms of ε^{54}Cr and Δ^{17}O indicates that they formed in the outer solar system from precursor material rich in refractory inclusions. This genetic relationship may also be supported by the observation of unidirectional paleomagnetism in CV chondrites, which suggests that they formed on a parent body that once had a liquid metallic core dynamo (Carporzen et al., 2011). To satisfy this feature, Elkins-Tanton et al. (2011) proposed a model in which the CV parent body was composed of an inner differentiated zone with a magma ocean capped by an undifferentiated CV/CK chondritic crust. As such, preservation of this chondritic crust is only feasible if the parent body formed with $^{26}Al/^{27}Al < 2 \times 10^{-5}$ (Elkins-Tanton et al., 2011).

The presence of refractory inclusions containing the canonical $^{26}Al/^{27}Al$ of 5.25×10^{-5} (Jacobsen et al., 2008; Larsen et al., 2011) in the CV precursor material for the Eagle Station parent body allows to estimate a conservative lower limit of the initial $(^{26}Al/^{27}Al)_0$. Addition of ~10 wt% refractory inclusions (comparable to the amount in CV chondrites; Krot et al., 2007) to initially ^{26}Al-poor disk solids ($^{26}Al/^{27}Al = 1.6 \times 10^{-5}$) results in a $(^{26}Al/^{27}Al)_0$ of $>2.7 \times 10^{-5}$ of this mixture at the time of CAI-formation. An upper limit of $^{26}Al/^{27}Al$ at 2×10^{-5} at the time of accretion of the CV parent body to preserve a chondritic crust therefore requires delayed formation at least 0.3 Myr post-CAIs (Fig. 9). Moreover, the lowest measured μ^{26}Mg* value of the olivine crystals requires onset of olivine formation within 1.75 Myr of CAI-formation (Fig. 4c). As such, this constrains the timing for onset of planetesimal accretion to within 0.3 to ~1.3 Myr post-CAIs (Fig. 9). This timeframe appears to be consistent with the ε^{182}W deficit of Eagle Station metal that imply metal–silicate differentiation ~1 Myr after solar system formation (Quitté et al., 2005).

Protracted accretion timescales in the outer protoplanetary disk are also supported by dynamical models for planetesimal formation. Owing to the progressive removal of gas, increasing dust/gas ratio and faster dynamical timescales, such models predict very rapid planetesimal accretion in inner disk regions with declining efficiency with orbital distance from the proto-Sun (Weidenschilling, 2000). Therefore, although the efficiency of the accretion process may vary locally, for example, due to the increased sticking efficiency of icy-particles beyond the snow-line (e.g. Blum and Wurm, 2008), planetesimal formation is generally predicted to proceed as a wave propagating outward through the disk. In summary,

as suggested by their ε^{54}Cr signatures, the very early accretion timescales (<250,000 years post-CAIs) inferred here for ε^{54}Cr and $(^{26}Al/^{27}Al)_0$ deficient planetesimals is consistent with an inner disk origin (Fig. 10). By extension, the delayed accretion timescales (0.3 to ~1 Myr post-CAIs) inferred for meteorite parent bodies, such as the CV/Eagle Station parent body with excess ε^{54}Cr, is predicted for an outer disk origin for these carbonaceous planetesimals. The presence of hydrated minerals in carbonaceous chondritic meteorites is evidence for the former presence of water ice on their parent bodies and supports their formation beyond the snowline (Morbidelli et al., 2012).

4.5.3 Formation of ungrouped pallasites; Zinder and Milton—The relatively high pyroxene content (28 vol%) of the ungrouped Zinder pallasite (Bunch et al., 2005) suggests an origin as solid residue from lower degrees of partial melting than those experienced by MGPs and pyroxene pallasites (<2 vol%). The similar Mg isotope composition of those pallasites further supports formation under similar conditions. The origin of the ungrouped Milton pallasite is, however, difficult to constrain because the oxygen isotope composition of its silicates suggests it originated on a separate parent body of carbonaceous chondrite-type of composition, yet distinct from both the parent bodies of MGPs and ESPs (Jones et al., 2003). If correct, similar to inferences drawn here from the Mg isotope composition of MGPs, the heavy Mg isotope composition of its olivine relative to carbonaceous chondrites (Fig. 1) may reflect an origin as a solid residue from high degrees of partial melting.

5 Conclusion

We have conducted a high-precision analysis of the Mg isotope composition of various types of high-temperature igneous products, including various pallasites that are believed to have formed on distinct parent bodies, as well as one primitive achondrite and undifferentiated chondritic meteorites. To constrain the accretion and differentiation timescales for asteroidal bodies in our solar system, these data are combined with thermal modeling for planetesimal melting using ^{26}Al as a heat source. We suggest that the efficiency of planetesimal formation processes is dependent on heliocentric distance and that the mineralogical and compositional diversity of the achondritic meteorites is best explained by significant differences in the initial ^{26}Al abundance between inner and outer protoplanetary disk. Our model for planetesimal formation bridges the formation timescales of differentiated and undifferentiated meteorites through continued accretion of early-formed planetesimals with partly differentiated onion-shell interior structures. We detail below the main results and interpretations from our study:

1. The mass-dependent Mg isotope composition (μ^{25}Mg) of the Eagle Station pallasite is identical to most chondritic meteorites, but resolvably lighter relative to the composition of Main Group Pallasites, pyroxene pallasites, the ungrouped Zinder and Milton pallasites as well as Earths mantle and CI chondrites. A component of this variability may result from the admixing of refractory inclusions with isotopically light compositions, such as amoeboid olivine aggregates, to the outer accretion disk regions of the Eagle Station parent body. The 63 ± 39 ppm/amu (2sd) heavier Mg isotope composition of Main Group Pallasites (as well as pyroxene

pallasites and primitive achondrites) relative to ordinary chondrites may be understood by extraction of an isotopically light partial melt composition from an olivine-rich solid residue.

2. The negative and restricted $\mu^{26}Mg^*$ recorded by Main Group Pallasite olivines, pyroxene pallasites, as well as primitive achondrites (lodranite, acapulcoite) further corroborate an origin as solid residues from high degrees of partial melting generated by heat production from ^{26}Al decay. Their $\mu^{26}Mg^*$ deficits seems to correlate with the degree of partial melting experienced by these meteorites. This indicates that the limited $\mu^{26}Mg^*$ variability in these rocks was generated by ^{26}Al decay and suggests a common temporal evolution linked to their magmatic genesis. Based on the intrinsic relationship between ^{26}Al decay and the thermal evolution of asteroidal bodies, we propose that these meteorites are the products of incomplete melting of rapidly accreting and partially differentiated large (>100 km) non-carbonaceous planetesimals with onion-shell structures consisting of olivine-rich zones of partial melting residues (such as Main Group and pyroxene pallasites, as well as primitive achondrites) capped by undifferentiated, partly metamorphosed chondritic crusts (e.g. ordinary chondrites). In this model, the chondritic crust was acquired through continuous accretion throughout the disk's lifetime (~3 Myr) and may in some cases have been penetrated by basaltic/pyroxenitic melts originating from the deeper olivinerich zones. We propose that these planetesimals formed throughout the hot (>500 K) inner protoplanetary disk characterized by a reduced initial $^{26}Al/^{27}Al_0$ ratio of $1–2 \times 10^{-5}$ relative to the canonical value. Onset of accretion and formation of such km-sized planetesimals occurred within ~250,000 years of solar system formation. Such rapid accretion timescale are in agreement with dynamical models for planetesimal formation. Furthermore, our model eliminates the need for a time-gap of ~2 Myr between onset of formation of large differentiated planetesimals and those of undifferentiated chondritic meteorites in the classical view of asteroid formation in our solar system, but instead reconciles their formation timescales within a unified model for continuous accretion of large partly differentiated planetesimals.

3. The variable and positive $\mu^{26}Mg^*$ recorded by olivines from the Eagle Station pallasite indicate an origin distinct from that of Main Group and pyroxene pallasites, plausibly as crystallization products of a large-scale differentiating magmatic reservoir associated with the igneous evolution of Eagle Station/CV-type parent bodies. In accordance with paleomagnetic evidence for an internal core dynamo within the CV parent body, we suggest that Eagle Station pallasites originated on partly differentiated carbonaceous planetesimals in the cool outer protoplanetary disk characterized by high initial $(^{26}Al/^{27}Al)_0$ of $>2.7 \times 10^{-5}$. Our analysis shows that such planetesimals started accreting 0.3–1 Myr post-CAIs and continued their quiescent accretion for several million years, thereby

Europe PMC Funders Author Manuscripts

acquiring a thick undifferentiated carbonaceous chondritic crust. Such delayed and protracted planetesimal accretion timescales in the outer disk are in accordance with dynamical models for planetesimal formation.

4. The ungrouped Zinder pallasite has irresolvable Mg isotope compositions from that of Main Group Pallasites and, thus, could have formed under similar magmatic conditions and timescales. The ungrouped Milton pallasite, on the other hand, may represent a partial melting residue on a carbonaceous chondrite-type of planetesimal.

5. Our model does not rely on an extended time frame for the onset of planetesimal formation during an early epoch of run-away accretion such as proposed for the Martian planetary embryo (Dauphas and Pourmand, 2011). Instead, we propose that most of the planetesimal seeds for the terrestrial planets were established within a few hundred thousand years after formation of the proto-Sun. Hence, proto-Earth most likely accreted a large fraction of partly differentiated planetesimals in the initial stages of planetary accretion.

Acknowledgements

Funding for this project was provided by grants from the Danish National Research Foundation (grant number DNRF97) and from the European Research Council (ERC Consolidator grant agreement 616027-STARDUST2ASTEROIDS) to M.B. We thank Henning Haack and Tim McCoy for providing samples of the Eagle Station (USNM2752, NHMD1890.419), Cold Bay (USNM633), Philips County (USNM1695), Giroux (USNM1574) and Milton (USNM7816) pallasites. We thank Ian Sanders and two anonymous reviewers for constructive reviews. Sara S. Russell is acknowledged for editorial handling and useful comments.

References

Amelin Y. U–Pb ages of angrites. Geochim Cosmochim Acta. 2008; 72:221–232.

Asphaug E. Growth and evolution of asteroids. Annu Rev Earth Planet Sci. 2009; 37:413–448.

Baker JA, Schiller M, Bizzarro M. ^{26}Al–^{26}Mg deficit dating ultramafic meteorites and silicate planetesimal differentiation in the early Solar System? Geochim Cosmochim Acta. 2012; 77:415–431.

Bigeleisen J, Mayer MG. Calculation of equilibrium constants for isotopic exchange reactions. J Chem Phys. 1947; 15:261.

Bizzarro M, Baker JA, Haack H. Mg isotope evidence for contemporaneous formation of chondrules and refractory inclusions. Nature. 2004; 431:275–278. [PubMed: 15372023]

Bizzarro M, Baker JA, Haack H, Lundgaard KL. Rapid timescales for accretion and melting of differentiated planetesimals inferred from ^{26}Al–^{26}Mg chronometry. Astrophys J. 2005; 632:L41–L44.

Bizzarro M, Paton C, Larsen KK, Schiller M, Trinquier A, Ulfbeck D. High-precision Mg-isotope measurements of terrestrial and extraterrestrial material by HR-MC-ICPMS—implications for the relative and absolute Mg-isotope composition of the bulk silicate Earth. J Anal At Spectrom. 2011; 26:565.

Blum J, Wurm G. The growth mechanisms of macroscopic bodies in protoplanetary disks. Annu Rev Astron Astr. 2008; 46:21–56.

Boesenberg JS, Delaney JS, Hewins RH. A petrological and chemical reexamination of Main Group pallasite formation. Geochim Cosmochim Acta. 2012; 89:134–158.

Boss, AP.; Ciesla, FJ. The solar nebula. Treatise on Geochemistry. Elsevier Ltd; 2014. p. 37-53.

Bourdon B, Tipper ET, Fitoussi C, Stracke A. Chondritic Mg isotope composition of the Earth. Geochim Cosmochim Acta. 2010; 74:5069–5083.

Bouvier A, Wadhwa M, Simon SB, Grossman L. Magnesium isotopic fractionation in chondrules from the Murchison and Murray CM2 carbonaceous chondrites. Meteorit Planet Sci. 2013; 48:339–353.

Bunch TE, Rumble D III, Wittke JH, Irving AJ. Pyroxene-rich pallasites Zinder and NWA 1911: not like the others. Meteorit Planet Sci Suppl. 2005; 40:5219.

Buseck PR. Pallasite meteorites – mineralogy, petrology and geochemistry. Geochim Cosmochim Acta. 1977; 41:711–740.

Carporzen L, Weiss BP, Elkins-Tanton LT, Shuster DL, Ebel D, Gattacceca J. Magnetic evidence for a partially differentiated carbonaceous chondrite parent body. Proc Natl Acad Sci. 2011; 108(16): 6386–6389.

Carslaw, HS.; Jaeger, JC. Conduction of Heat in Solids. second ed. Clarendon Press; Oxford: 1959.

Castillo-Rogez J, Johnson TV, Lee MH, Turner NJ, Matson DL, Lunine J. ^{26}Al decay: heat production and a revised age for Iapetus. Icarus. 2009; 204:658–662.

Chakrabarti R, Jacobsen SB. The isotopic composition of magnesium in the inner Solar System. Earth Planet Sci Lett. 2010; 293:349–358.

Chambers JE. Planetary accretion in the inner Solar System. Earth Planet Sci Lett. 2004; 223:241–252.

Chambers J. Meteoritic diversity and planetesimal formation. Meteorites and the early solar system II. 2006:487–497.

Ciesla FJ. Radial transport in the solar nebula: implications for moderately volatile element depletions in chondritic meteorites. Meteorit Planet Sci. 2008; 43:639–655.

Clayton RN, Mayeda TK. Oxygen isotope studies of achondrites. Geochim Cosmochim Acta. 1996; 60:1999–2017.

Connelly JN, Bizzarro M, Thrane K, Baker JA. The Pb–Pb age of Angrite SAH99555 revisited. Geochim Cosmochim Acta. 2008; 72:4813–4824.

Connelly JN, Bizzarro M, Krot AN, Nordlund Å, Wielandt D, Ivanova MA. The absolute chronology and thermal processing of solids in the solar protoplanetary disk. Science. 2012; 338:651–655. [PubMed: 23118187]

Cournède C, Gattacceca J, Rochette P, Weiss B. Insights on asteroid partial differentiation and early solar system magnetic fields revealed by paleomagnetism of carbonaceous chondrites. LPI Contrib. 2014; 1800:5292.

Cuzzi JN, Hogan RC, Shariff K. Toward planetesimals: dense chondrule clumps in the protoplanetary nebula. Astrophys J. 2008; 687:1432.

Dauphas N, Pourmand A. Hf-W-Th evidence for rapid growth of Mars and its status as a planetary embryo. Nature. 2011; 473:489–492. [PubMed: 21614076]

Davis AM, Richter FM. Condensation and evaporation of solar system materials. Treatise Geochem. 2007; 1:407–430.

DeMeo FE, Carry B. Solar System evolution from compositional mapping of the asteroid belt. Nature. 2014; 505:629–634. [PubMed: 24476886]

Dodd, RT. Meteorites, A Petrologic-Chemical Synthesis. Cambridge University Press; 1981.

Dubrovinskaia N, Dubrovinsky L, Kantor I, Crichton W, Dmitriev V, Prakapenka V, Shen G, Vitos L, Ahuja R, Johansson B, Abrikosov I. Beating the miscibility barrier between iron group elements and magnesium by high-pressure alloying. Phys Rev Lett. 2005; 95:245502. [PubMed: 16384393]

Elkins-Tanton LT, Weiss BP, Zuber MT. Chondrites as samples of differentiated planetesimals. Earth Planet Sci Lett. 2011; 305:1–10.

Ferguson JM. Al26 decay scheme. Phys Rev. 1958; 112:1238–1240.

Fitoussi C, Bourdon B, Kleine T, Oberli F, Reynolds BC. Si isotope systematics of meteorites and terrestrial peridotites: implications for Mg/Si fractionation in the solar nebula and for Si in the Earth's core. Earth Planet Sci Lett. 2009; 287:77–85.

Fu RR, Elkins-Tanton LT. The fate of magmas in planetesimals and the retention of primitive chondritic crusts. Earth Planet Sci Lett. 2014; 390:128–137.

Galy A, Yoffe O, Janney PE, Williams RW, Cloquet C, Alard O, Halicz L, Wadhwa M, Hutcheon ID, Ramon E, Carignan J. Magnesium isotope heterogeneity of the isotopic standard SRM980 and new

Europe PMC Funders Author Manuscripts

reference materials for magnesium-isotope-ratio measurements. J Anal At Spectrom. 2003; 18:1352.

Georg RB, Halliday AN, Schauble EA, Reynolds BC. Silicon in the Earth's core. Nature. 2007; 447:1102–1106. [PubMed: 17597757]

Ghosh A, McSween HY Jr. A thermal model for the differentiation of asteroid 4 Vesta, based on radiogenic heating. Icarus. 1998; 134:187–206.

Ghosh A, Weidenschilling SJ, McSween HY Jr, Rubin A. Asteroidal heating and thermal stratification of the asteroid belt. Meteorites and the early solar system II. 2006:555–566.

Gradie J, Tedesco E. Compositional structure of the asteroid belt. Science. 1982; 216:1405–1407. [PubMed: 17798362]

Haack H, McCoy TJ. Iron and stony-iron meteorites. Treatise Geochem. 2007; 1:325–345.

Handler MR, Baker JA, Schiller M, Bennett VC, Yaxley GM. Magnesium stable isotope composition of Earth's upper mantle. Earth Planet Sci Lett. 2009; 282:306–313.

Henderson GS, Calas G, Stebbins JF. The structure of silicate glasses and melts. Elements. 2006; 2:269–273.

Henke S, Gail HP, Trieloff M, Schwarz WH. Thermal evolution model for the H chondrite asteroid - instantaneous formation versus protracted accretion. Icarus. 2013; 226:212–228.

Herndon JM. Substructure of the inner core of the Earth. Proc Natl Acad Sci. 1996; 93:646–648. [PubMed: 11607625]

Hess, PC. Origins of Igneous Rocks. Harvard University Press; Cambridge, MA: 1989.

Hevey PJ, Sanders IS. A model for planetesimal meltdown by ^{26}Al and its implications for meteorite parent bodies. Meteorit Planet Sci. 2006; 41:95–106.

Huang F, Zhang Z, Lundstrom CC, Zhi X. Iron and magnesium isotopic compositions of peridotite xenoliths from Eastern China. Geochim Cosmochim Acta. 2011; 75:3318–3334.

Hutchison, R. Meteorites: A Petrologic, Chemical and Isotopic Synthesis. Cambridge University Press; 2004.

Johansen A, Oishi JS, Low M-MM, Klahr H, Henning T, Youdin A. Rapid planetesimal formation in turbulent circumstellar disks. Nature. 2007; 448:1022–1025. [PubMed: 17728751]

Jacobsen B, Yin Q-Z, Moynier F, Amelin Y, Krot AN, Nagashima K, Hutcheon ID, Palme H. ^{26}Al–^{26}Mg and ^{207}Pb–^{206}Pb systematics of Allende CAIs: canonical solar initial ^{26}Al/^{27}Al ratio reinstated. Earth Planet Sci Lett. 2008; 272:353–364.

Johansen A, Mac Low M-M, Lacerda P, Bizzarro M. Growth of asteroids, embryos and Kuiper belt objects by chondrule accretion. Sci Adv. 2015; 1:e1500109. [PubMed: 26601169]

Jones RH, Wasson JT, Larson T, Sharp ZD. Milton: a new, unique pallasite. Lunar Planet Inst Sci Conf Abstr. 2003; 34:1683.

Kádas K, Vitos L, Johansson B, Ahuja R. Stability of body-centered cubic iron–magnesium alloys in the Earth's inner core. Proc Natl Acad Sci. 2009; 106:15560–15562. [PubMed: 19805214]

Kleine T, Touboul M, Van Orman JA, Bourdon B. Hf–W thermochronometry: closure temperature and constraints on the accretion and cooling history of the H chondrite parent body. Earth Planet Sci Lett. 2008; 270:106–118.

Kleine T, Hans U, Irving AJ, Bourdon B. Chronology of the angrite parent body and implications for core formation in protoplanets. Geochim Cosmochim Acta. 2012; 84:186–203.

Koefoed, P.; Amelin, Y.; Yin, Q-Z.; Sanborn, ME.; Huyskens, M. 46th Lunar and Planetary Science Conference; Houston: Lunar and Planetary Institute; 2015. p. 1842

Kroeker S, Stebbins JF. Magnesium coordination environments in glasses and minerals: new insight from high-field magnesium-25 MAS NMR. Am Mineral. 2000; 85:1459–1464.

Krot AN, Keil K, Scott ERD. Classification of meteorites. Treatise Geochem. 2007; 1:83.

Kruijer TS, Touboul M, Fischer-Godde M, Bermingham KR, Walker RJ, Kleine T. Protracted core formation and rapid accretion of protoplanets. Science. 2014; 344:1150–1154. [PubMed: 24904163]

Larsen KK, Trinquier A, Paton C, Schiller M, Wielandt D, Ivanova MA, Connelly JN, Nordlund Å, Krot AN, Bizzarro M. Evidence for magnesium isotope heterogeneity in the solar protoplanetary disk. Astrophys J. 2011; 735:L37.

Lee T, Papanastassiou DA, Wasserburg GJ. Demonstration of ^{26}Mg excess in Allende and evidence for ^{26}Al. Geophys Res Lett. 1976; 3:41–44.

Liu S-A, Teng F-Z, Yang W, Wu F-Y. High-temperature inter-mineral magnesium isotope fractionation in mantle xenoliths from the North China craton. Earth Planet Sci Lett. 2011; 308:131–140.

Lodders, K.; Fegley, B, Jr. The Planetary Scientist's Companion. Oxford University Press; 1998. p. 1-392.

Luu T-H, Chaussidon M, Birck J-L. Timing of metal–silicate differentiation in the Eagle Station pallasite parent body. CR Geosci. 2014; 346:75–81.

MacPherson GJ, Davis AM, Zinner EK. The distribution of aluminum-26 in the early Solar System—a reappraisal. Meteorit Planet Sci. 1995; 30:365–386.

MacPherson GJ, Kita NT, Ushikubo T, Bullock ES, Davis AM. Well-resolved variations in the formation ages for Ca–Al-rich inclusions in the early Solar System. Earth Planet Sci Lett. 2012; 331–332:43–54.

Mare ER, Tomkins AG, Godel BM. Restriction of parent body heating by metal-troilite melting: thermal models for the ordinary chondrites. Meteorit Planet Sci. 2014; 49:636–651.

McCoy TJ, Keil K, Muenow DW, Wilson L. Partial melting and melt migration in the acapulcoite-lodranite parent body. Geochim Cosmochim Acta. 1997; 61:639–650.

McCoy TJ, Mittlefehldt DW, Wilson L. Asteroid differentiation. Meteorites and the early solar system II. 2006

Mittlefehldt DW, Lindstrom MM, Bogard DD, Garrison DH, Field SW. Acapulco- and Lodran-like achondrites: petrology, geochemistry, chronology, and origin. Geochim Cosmochim Acta. 1996; 60:867–882.

Mittlefehldt DW, McCoy TJ, Goodrich CA, Kracher A. Non-chondritic meteorites from asteroidal bodies. Reviews in Mineralogy and Geochemistry. 1998:4.1–1.195.

Monnereau M, Toplis MJ, Baratoux D, Guignard J. Thermal history of the H-chondrite parent body: implications for metamorphic grade and accretionary time-scales. Geochim Cosmochim Acta. 2013; 119:302–321.

Morbidelli A, Bottke WF, Nesvorný D, Levison HF. Asteroids were born big. Icarus. 2009; 204:558–573.

Morbidelli A, Lunine JI, O'Brien DP, Raymond SN, Walsh KJ. Building Terrestrial Planets. Annu Rev Earth Planet Sci. 2012; 40:251–275.

Moskovitz N, Gaidos E. Differentiation of planetesimals and the thermal consequences of melt migration. Meteorit Planet Sci. 2011; 46:903–918.

Mysen, BO.; Richet, P. Silicate glasses and melts: properties and structure. Developments in Geochemistry. Elsevier; 2005. p. 560

Nakamura T, Noguchi T, Tanaka M, Zolensky ME, Kimura M, Tsuchiyama A, Nakato A, Ogami T, Ishida H, Uesugi M, Yada T, et al. Itokawa dust particles: a direct link between S-type asteroids and ordinary chondrites. Science. 2011; 333:1113–1116. [PubMed: 21868667]

Nesse, WD. Introduction to Mineralogy. Oxford University Press; 2000.

Neumann W, Breuer D, Spohn T. Differentiation of Vesta: implications for a shallow magma ocean. Earth Planet Sci Lett. 2014; 395:267–280.

Paton C, Hellstrom J, Paul B, Woodhead J, Hergt J. Iolite: freeware for the visualisation and processing of mass spectrometric data. J Anal At Spectrom. 2011; 26:2508.

Paton C, Schiller M, Bizzarro M. Identification of an 84 Sr-depleted carrier in primitive meteorites and implications for thermal processing in the solar protoplanetary disk. Astrophys J. 2013; 763:L40.

Pfalzner S, Davies MB, Gounelle M, Johansen A, Muenker C, Lacerda P, Zwart SP, Testi L, Trieloff M, Veras D. The formation of the solar system. Phys Scr. 2015:068001.

Pogge von Strandmann PAE, Elliott T, Marschall HR, Coath C, Lai Y-J, Jeffcoate AB, Ionov DA. Variations of Li and Mg isotope ratios in bulk chondrites and mantle xenoliths. Geochim Cosmochim Acta. 2011; 75:5247–5268.

Poitrasson F, Levasseur S, Teutsch N. Significance of iron isotope mineral fractionation in pallasites and iron meteorites for the core–mantle differentiation of terrestrial planets. Earth Planet Sci Lett. 2005; 234:151–164.

Quitté G, Birck J-L, Allègre CJ. Stony-iron meteorites: history of the metal phase according to tungsten isotopes. Geochim Cosmochim Acta. 2005; 69:1321–1332.

Sanders IS, Scott ERD. The origin of chondrules and chondrites: debris from low-velocity impacts between molten planetesimals? Meteorit Planet Sci. 2012; 47:2170–2192.

Sahijpal S, Gupta G. Did the carbonaceous chondrites evolve in the crustal regions of partially differentiated asteroids? J Geophys Res. 2011; 116:E06004.

Sahijpal S, Soni P, Gupta G. Numerical simulations of the differentiation of accreting planetesimals with ^{26}Al and ^{60}Fe as the heat sources. Meteorit Planet Sci. 2007; 42:1529–1548.

Schauble EA. Applying stable isotope fractionation theory to new systems. Rev Mineral Geochem. 2004; 55:65–111.

Schauble EA. First-principles estimates of equilibrium magnesium isotope fractionation in silicate, oxide, carbonate and hexaaquamagnesium(2+) crystals. Geochim Cosmochim Acta. 2011; 75:844–869.

Schiller M, Baker JA, Bizzarro M. ^{26}Al–^{26}Mg dating of asteroidal magmatism in the young Solar System. Geochim Cosmochim Acta. 2010; 74:4844–4864.

Schiller M, Baker J, Creech J, Paton C, Millet M-A, Irving A, Bizzarro M. Rapid timescales for magma ocean crystallization on the Howardite–Eucrite–Diogenite parent body. Astrophys J. 2011; 740:L22.

Schiller M, Connelly JN, Clad AC, Mikouchi T, Bizzarro M. Early accretion of protoplanets inferred from a reduced inner solar system ^{26}Al inventory. Earth Planet Sci Lett. 2015a; 420:45–54. [PubMed: 27429474]

Schiller M, Paton C, Bizzarro M. Evidence for nucleosynthetic enrichment of the protosolar molecular cloud core by multiple supernova events. Geochim Cosmochim Acta. 2015b; 149:88–102. [PubMed: 25684790]

Schramm DN, Tera F, Wasserburg GJ. The isotopic abundance of ^{26}Mg and limits on ^{26}Al in the early solar system. Earth Planet Sci Lett. 1970; 10:44–59.

Scott ER. Formation of olivine-metal textures in pallasite meteorites. Geochim Cosmochim Acta. 1977; 41:693–710.

Scott E, Krot AN. Chondrites and their components. Treatise Geochem. 2007; 1:143–200.

Shukolyukov A, Lugmair G. Manganese–chromium isotope systematics of carbonaceous chondrites. Earth Planet Sci Lett. 2006; 250:200–213.

Tang H, Dauphas N. ^{60}Fe–^{60}Ni chronology of core formation in Mars. Earth Planet Sci Lett. 2014; 390:264–274.

Tarduno JA, Cottrell RD, Nimmo F, Hopkins J, Voronov J, Erickson A, Blackman E, Scott ERD, McKinley R. Evidence for a dynamo in the main group pallasite parent body. Science. 2012; 338:939–942. [PubMed: 23161997]

Teng F-Z, Li W-Y, Ke S, Marty B, Dauphas N, Huang S, Wu F-Y, Pourmand A. Magnesium isotopic composition of the Earth and chondrites. Geochim Cosmochim Acta. 2010; 74:4150–4166.

Touboul M, Kleine T, Bourdon B, Van Orman JA, Maden C, Zipfel J. Hf–W thermochronometry: II. Accretion and thermal history of the acapulcoite–lodranite parent body. Earth Planet Sci Lett. 2009; 284:168–178.

Trieloff M, et al. Structure and thermal history of the H-chondrite parent asteroid revealed by thermochronometry. Nature. 2003; 422:500–502. [PubMed: 12673244]

Trinquier A, Birck J-L, Allègre CJ. Widespread ^{54}Cr heterogeneity in the inner solar system. Astrophys J. 2007; 655:1179.

Trinquier A, Elliott T, Ulfbeck D, Coath C, Krot AN, Bizzarro M. Origin of nucleosynthetic isotope heterogeneity in the solar protoplanetary disk. Science. 2009; 324:374–376. [PubMed: 19372428]

Urey HC. The thermodynamic properties of isotopic substances. J Chem Soc. 1947:562–581. (Resumed). [PubMed: 20249764]

Villeneuve J, Chaussidon M, Libourel G. Magnesium isotopes constraints on the origin of Mg-rich olivines from the Allende chondrite: nebular versus planetary? Earth Planet Sci Lett. 2011; 301:107–116.

Walsh KJ, Morbidelli A, Raymond SN, O'Brien DP, Mandell AM. A low mass for Mars from Jupiter's early gas-driven migration. Nature. 2011; 475:206–209. [PubMed: 21642961]

Warren PH. Stable-isotopic anomalies and the accretionary assemblage of the Earth and Mars: a subordinate role for carbonaceous chondrites. Earth Planet Sci Lett. 2011; 311:93–100.

Wasserburg GJ, Wimpenny J, Yin Q-Z. Mg isotopic heterogeneity, Al–Mg isochrons, and canonical $^{26}Al/^{27}Al$ in the early solar system. Meteorit Planet Sci. 2012; 47:1980–1997.

Wasson JT, Choi B-G. Main-group pallasites. Geochim Cosmochim Acta. 2003; 67:3079–3096.

Weidenschilling SJ. Formation of planetesimals and accretion of the terrestrial planets. Space Sci Rev. 2000; 92:295–310.

Weidenschilling SJ. Accretion of planetary embryos in the inner and outer solar system. Phys Scr T. 2008; 130:014021.

Weiss BP, Elkins-Tanton LT. Differentiated planetesimals and the parent bodies of chondrites. Annu Rev Earth Planet Sci. 2013; 41:529–560.

White, WM. Geochemistry. Wiley-Blackwell: 2013.

Williams JP, Cieza LA. Protoplanetary disks and their evolution. Ann Rev Astron Astrophys. 2011; 49:67–117.

Yang J, Goldstein JI, Scott ERD. Main-group pallasites: thermal history, relationship to IIIAB irons, and origin. Geochim Cosmochim Acta. 2010; 74:4471–4492.

Young ED, Tonui E, Manning CE, Schauble E, Macris CA. Spinel–olivine magnesium isotope thermometry in the mantle and implications for the Mg isotopic composition of Earth. Earth Planet Sci Lett. 2009; 288:524–533.

Europe PMC Funders Author Manuscripts

Europe PMC Funders Author Manuscripts

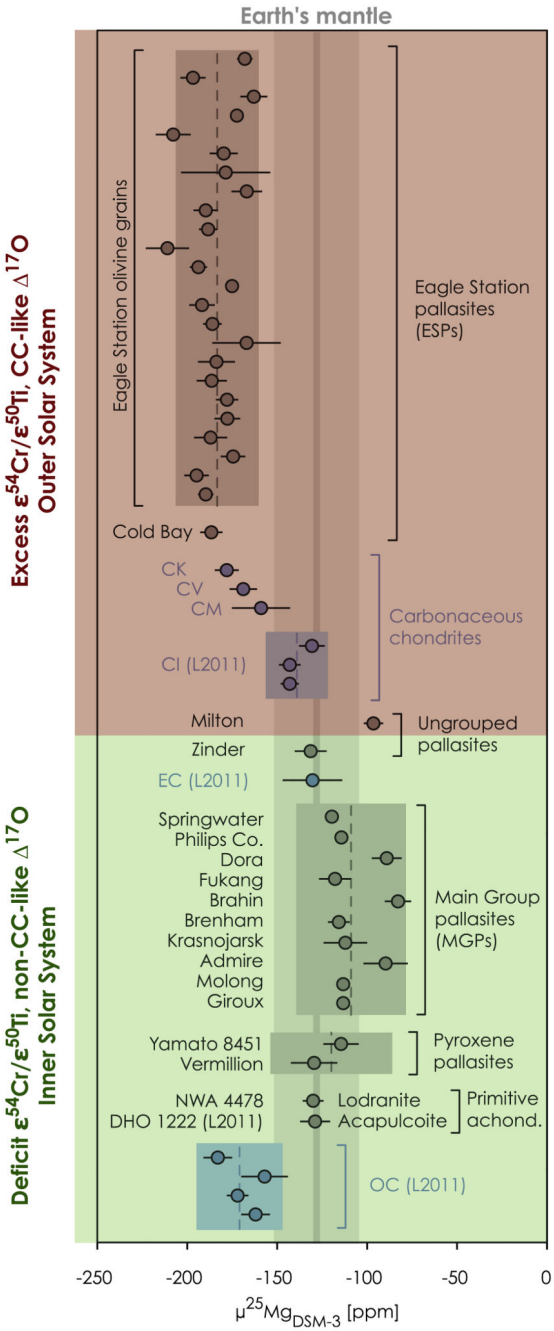

Fig. 1.

$\mu^{25}Mg$ of pallasites, primitive achondrites and chondrites (blue) reported as the parts per millions deviations from the terrestrial standard DSM-3. Also shown are Mg isotope data for Earth's mantle (light gray box, [−128 ± 23 (2sd) ppm]; average calculated from pristine mantle peridotites and olivines from Young et al., 2009; Handler et al., 2009; Bourdon et al., 2010; Schiller et al., 2010; Teng et al., 2010; Huang et al., 2011; Liu et al., 2011; Pogge von Strandmann et al., 2011). Data for CI chondrites (Orgueil; Alais; Ivuna), ordinary chondrites (OC; Kramer Creek [L4]; Tennasilm [L4]; Barratta [L3.8]; Heredia [H5]), one enstatite

chondrite (EC; SAH 97159 [EH3]) and the acapulcoite (DHO 1222) are from Larsen et al., 2011 (L2011). Gray shades represent weighted averages and their associated uncertainties (2sd). Error bars for individual samples represent the internal errors (2se).

Europe PMC Funders Author Manuscripts

Europe PMC Funders Author Manuscripts

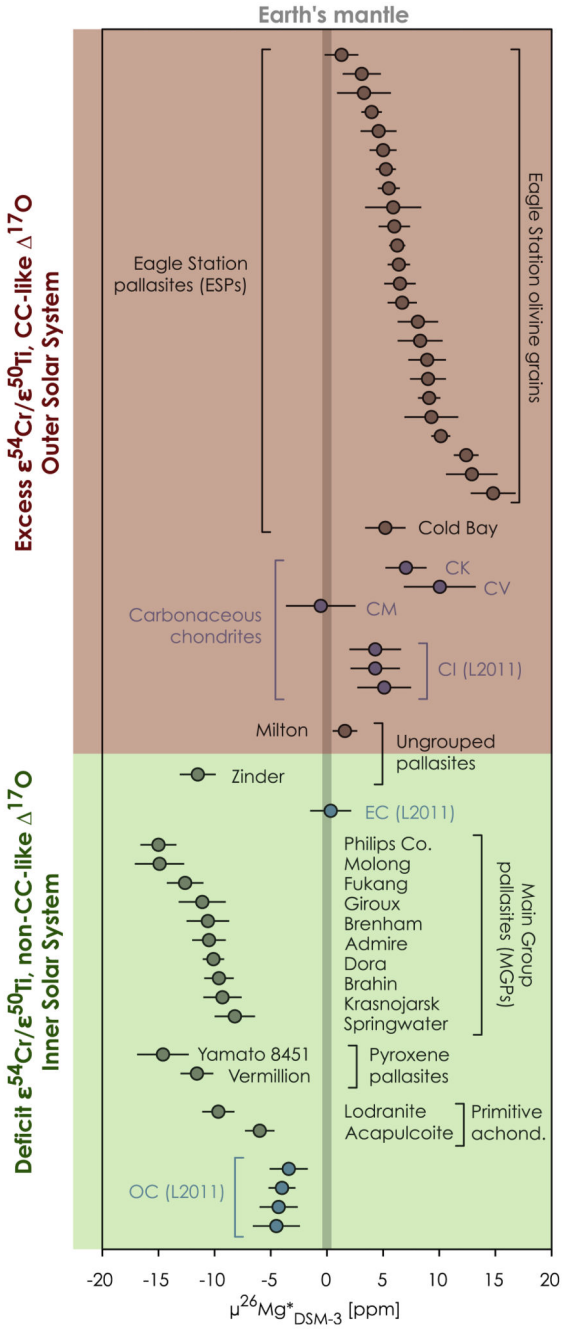

Fig. 2.

Mass-independent Mg isotope compositions ($\mu^{26}Mg^*$) for pallasites, primitive achondrites and chondrites (blue) reported as the parts per millions deviations from the terrestrial standard DSM-3. Data for CI chondrites (Orgueil; Alais; Ivuna), ordinary chondrites (OC; Kramer Creek [L4]; Tennasilm [L4]; Barratta [L3.8]; Heredia [H5]), one enstatite chondrite (EC; SAH 97159 [EH3]) and the acapulcoite (DHO 1222) are from Larsen et al., 2011 (L2011). Error bars for individual samples are represented by the internal errors (2se).

Europe PMC Funders Author Manuscripts

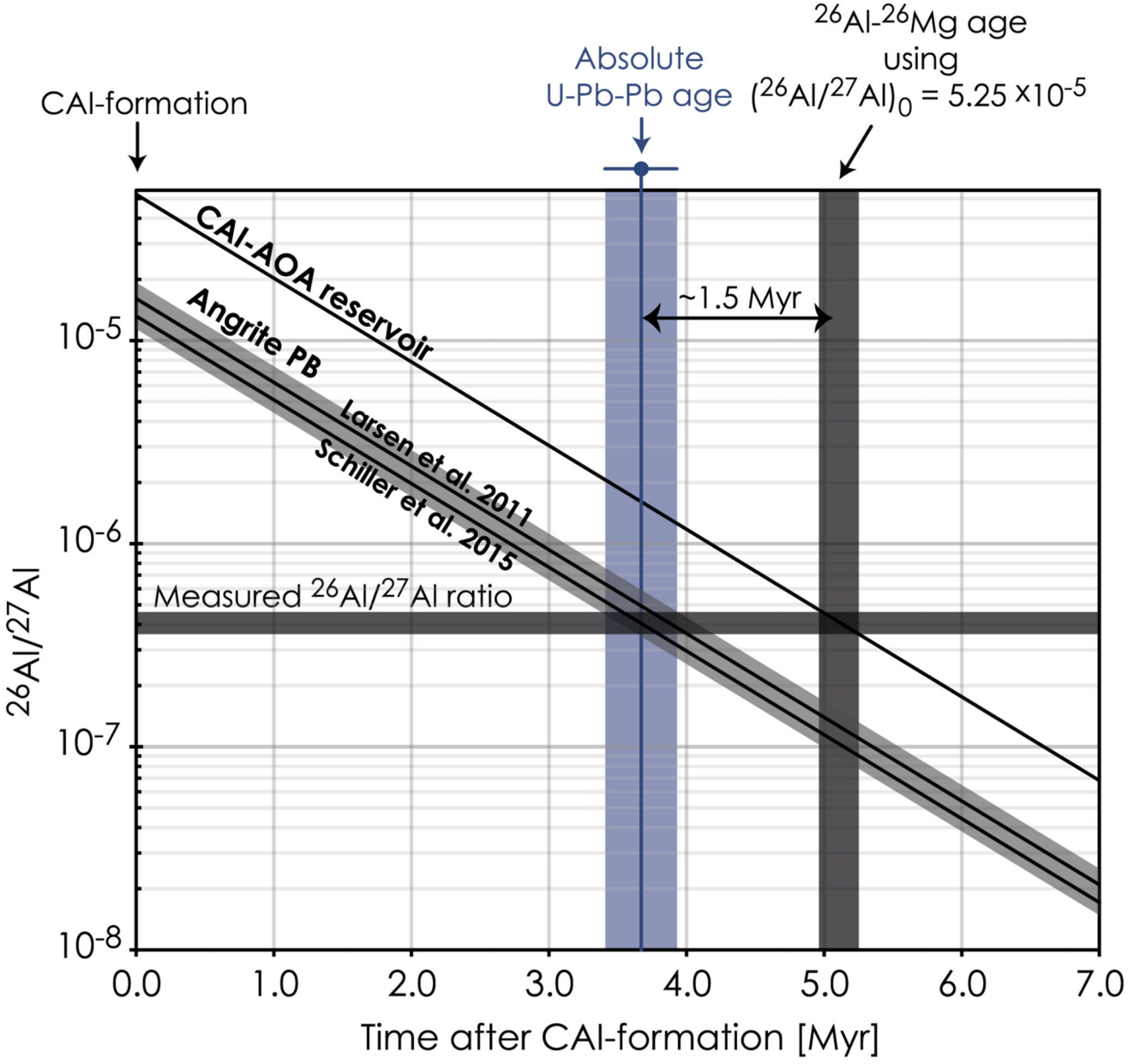

Fig. 3.

^{26}Al evolution diagram expressing the logarithmic ^{26}Al/^{27}Al ratio as a function of time after CAI-formation. Slopes correspond to $-\lambda t$, where λ represents the ^{26}Al decay constant (9.5×10^{-7} year^{-1}) and t is time. The intercepts correspond to initial $(^{26}\mathrm{Al}/^{27}\mathrm{Al})_0$ ratio at the time of CAI-formation. The diagram shows the ~1.5 Myr age discrepancy between relative ^{26}Al–^{26}Mg ages (Schiller et al., 2010, 2015a) and absolute U-corrected Pb–Pb ages (Larsen et al., 2011) of the rapidly cooled basaltic angrite meteorite SAH 99555 when using the canonical initial $(^{26}\mathrm{Al}/^{27}\mathrm{Al})_0$ of 5.25×10^{-5} defined by refractory inclusions (CAIs and AOAs) in CV chondrites (Jacobsen et al., 2008; Larsen et al., 2011). This age discrepancy is

eliminated when using a reduced initial $(^{26}Al/^{27}Al)_0$ as defined for the angrite parent body (Larsen et al., 2011 [1.6×10^{-5}]; Schiller et al., 2015a [1.3×10^{-5}]). PB = Parent Body.

Europe PMC Funders Author Manuscripts

Europe PMC Funders Author Manuscripts

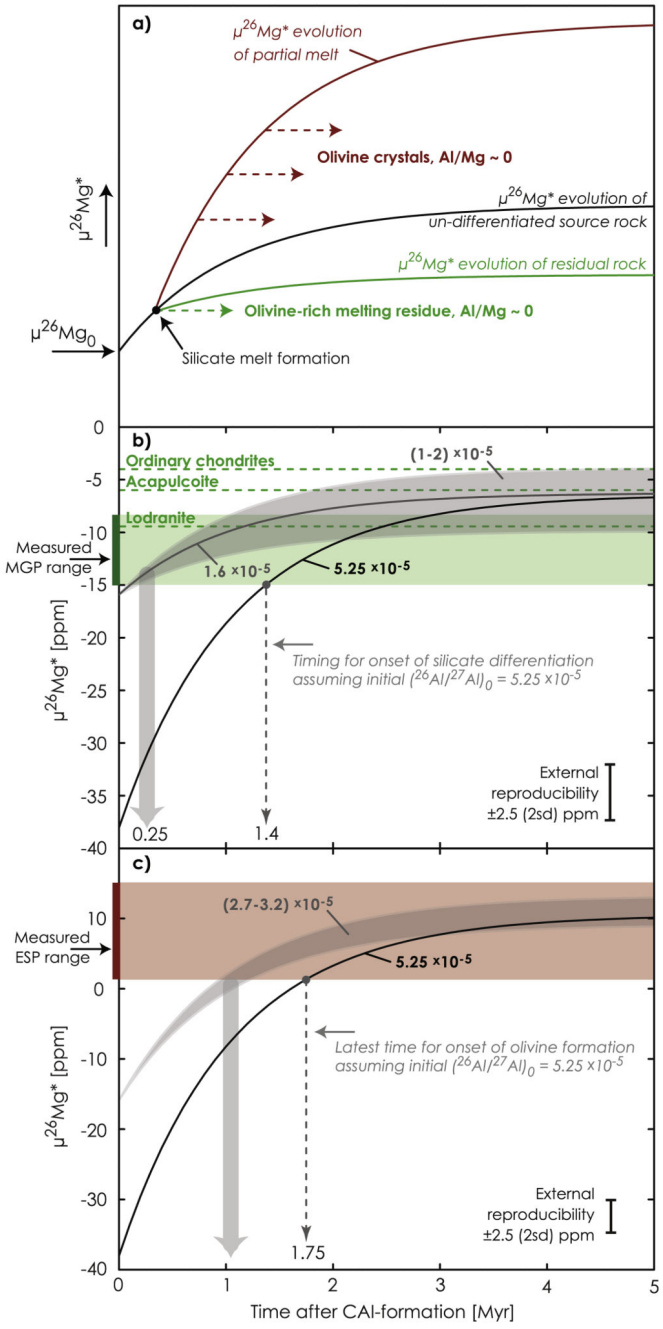

Fig. 4.

μ^{26}Mg* evolution diagrams showing the radiogenic ingrowth of ^{26}Mg* from ^{26}Al decay. **(a)** Schematics of the predicted μ^{26}Mg* evolution of source reservoirs (melt [red], residue [green] and undifferentiated source rock [black]) generated by magmatic differentiation. Retarded ingrowth of ^{26}Mg* in the residual rock ($Al/Mg_{residue} \ll Al/Mg_{source\ rock}$) results from extraction of an Al-rich partial melt. **(b)** μ^{26}Mg* ingrowth in an ordinary chondrite type of protolith ($^{27}Al/^{24}Mg = 0.084$) using either the canonical $(^{26}Al/^{27}Al)_0$ of 5.25×10^{-5} and initial $\mu^{26}Mg_0 = -38$ ppm (black curve) or a reduced initial $(^{26}Al/^{27}Al)_0$ of $1-2 \times 10^{-5}$

and $\mu^{26}Mg_0$ of −15.9 ppm (Larsen et al., 2011) (gray shades). The $\mu^{26}Mg^*$ deficits recorded by Main Group, pyroxene, and the ungrouped Zinder pallasites, as well as primitive achondrites is expected for retarded $\mu^{26}Mg^*$ ingrowth in a residue. The lowest MGP $\mu^{26}Mg^*$ value constrains the onset of silicate differentiation to ~ 1.4 Myr after CAI-formation using the canonical $(^{26}Al/^{27}Al)_0$ or to ~0.25 Myr using a reduced $(^{26}Al/^{27}Al)_0$. **(c)** $\mu^{26}Mg^*$ ingrowth in a CV carbonaceous chondrite protolith ($^{27}Al/^{24}Mg = 0.129$) using either the canonical $(^{26}Al/^{27}Al)_0$ or a reduced $(^{26}Al/^{27}Al)_0$ of $2.7–3.2 \times 10^{-5}$ (upper bound constrained by the CV bulk $\mu^{26}Mg^*$ value (incl. error); Table 2). The latest time for onset of ESP olivine formation is within ~1.75 Myr post-CAIs assuming canonical $(^{26}Al/^{27}Al)_0$ or ~1 Myr for a reduced $(^{26}Al/^{27}Al)_0$. Formation of ESP through crystallization will change the Al/Mg ratio of the source melt only slightly and thus lower the formation timescales.

Europe PMC Funders Author Manuscripts

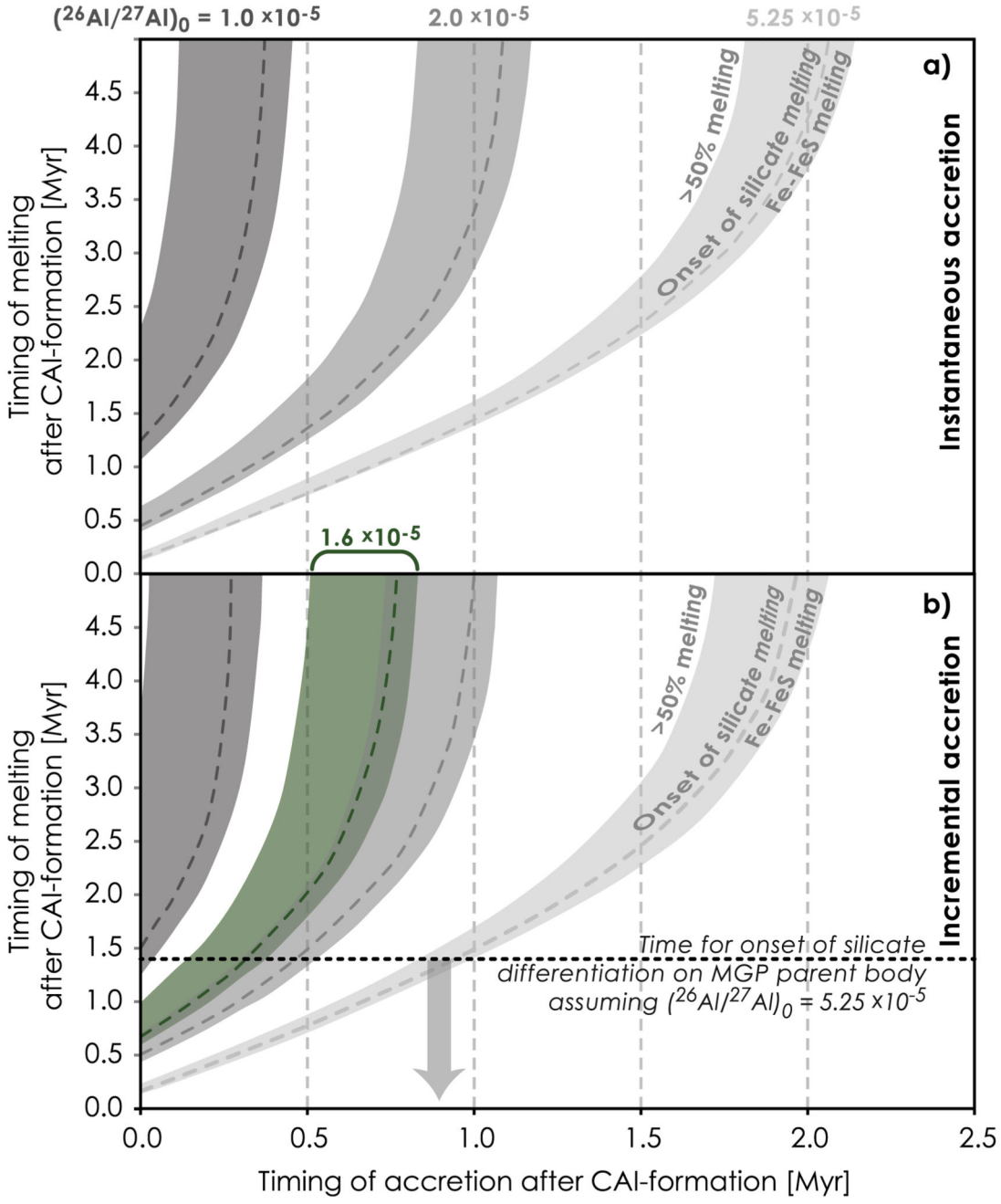

Fig. 5.

Thermal evolution diagrams showing the heating profiles within the centre of a large (100 km in radius) planetesimal of ordinary chondrite-type of composition. The ambient disk temperature is assumed constant at 250 K. (a and b) Timing of melting versus timing of accretion, assuming (a) instantaneous accretion and (b) incremental accretion. Temperature profiles are shown for a 'canonical' initial $(^{26}Al/^{27}Al)_0$ of 5.25×10^{-5} and for a reduced initial $(^{26}Al/^{27}Al)_0$ in the range $1-2 \times 10^{-5}$.

Europe PMC Funders Author Manuscripts

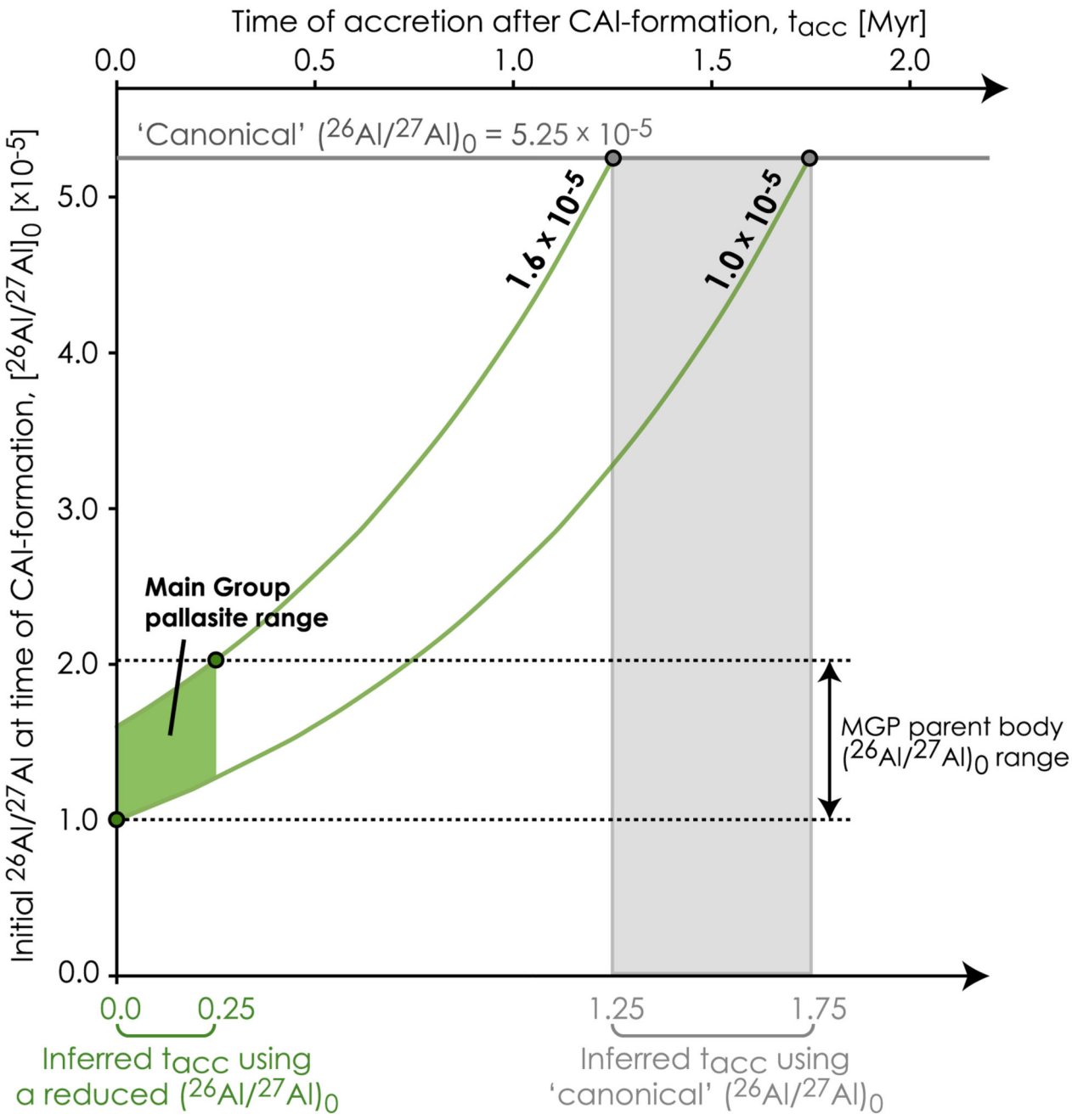

Fig. 6.

^{26}Al decay diagram showing the initial $(^{26}Al/^{27}Al)_0$ at the time of CAI-formation versus accretion time. Curves represent $^{26}Al/^{27}Al$ at the time of accretion. Early formation (<250 kyr) of the Main Group Pallasite (MGP) parent body as constrained by a reduced initial $(^{26}Al/^{27}Al)_0$ in the range $1-2 \times 10^{-5}$ translates into $^{26}Al/^{27}Al$ ratios at the time of accretion of $1-1.6 \times 10^{-5}$. Extrapolating this $^{26}Al/^{27}Al$ range to a 'canonical' initial $(^{26}Al/^{27}Al)_0$ ratio of 5.25×10^{-5} results in a late formation within 1.25−1.75 Myr after CAI-formation.

Europe PMC Funders Author Manuscripts

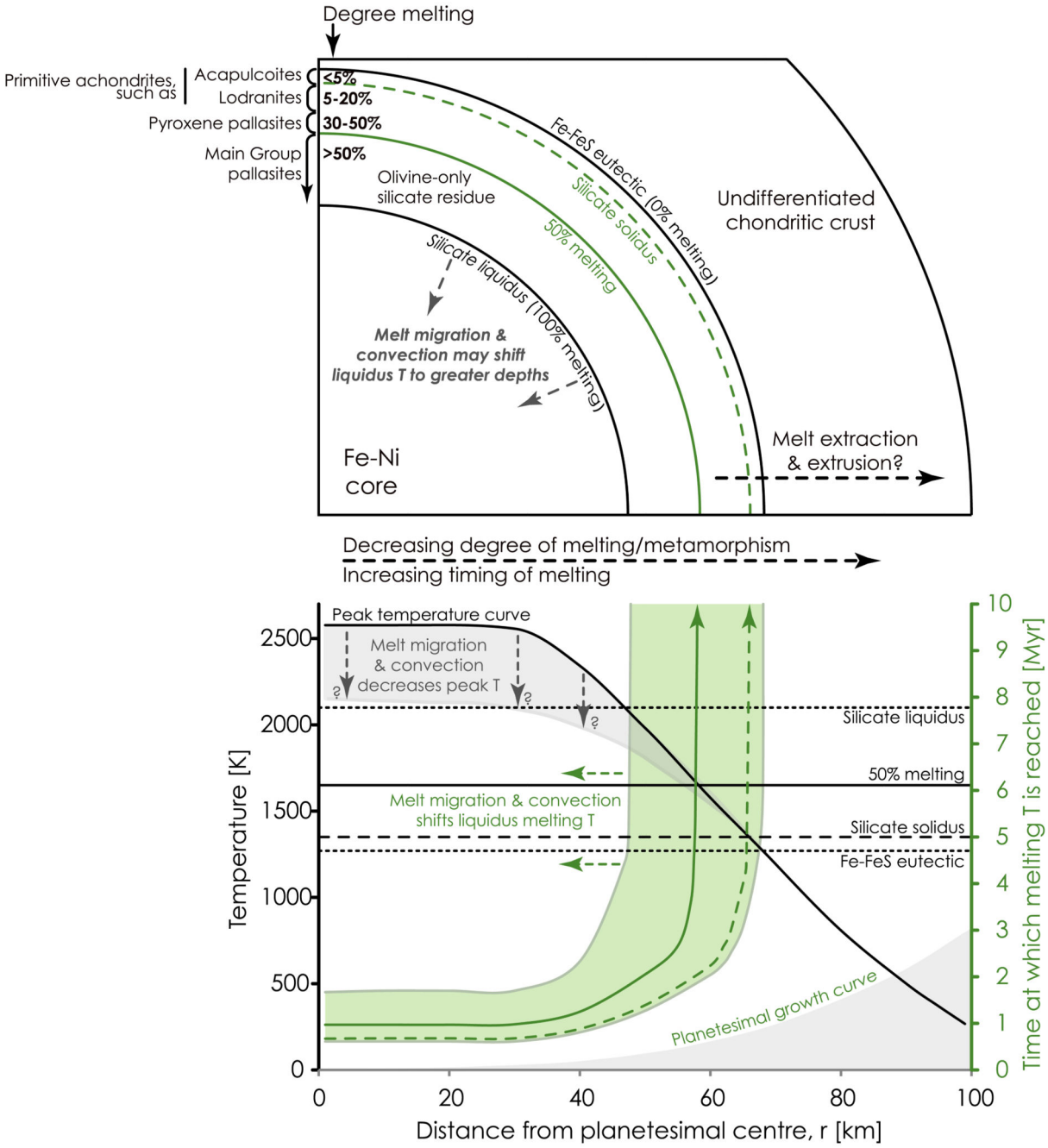

Fig. 7.

Thermal evolution for the heating stage for an ordinary chondrite-type of planetesimal that forms with a reduced $^{26}Al/^{27}Al$ ratio of 1.6×10^{-5} and accretes to a final radius of 100 km in 3 Myr. Heating profiles are shown as a function of distance from the planetesimal centre. Black curves represent temperatures, whereas green curves represent the time at which a given melting temperature is reached as a function of distance. The ambient disk temperature was assumed constant at 250 K. The green area represents the region within the planetesimal that experiences only partial melting of the source rock. This region progresses

outwards as accretion proceeds. The heating profiles are not significantly influenced by heat loss through convection up to about 50% melting (McCoy et al., 2006). As such, the liquidus temperature curve may progress towards the planetesimal centre when melt migration and convection becomes faster than the heating rate. The top sketch shows a cross-section through the final onion-shell structure of the partially differentiated planetesimal, which consists of an inner Fe-Ni core overlaid bya partial melting zone comprised of olivine-rich residues produced through basaltic/pyroxenitic melt extraction. The partial melting zone is dominated by progressively more olivine-rich silicate residues towards the interior and could be represented by meteorites such as Main Group Pallasites (>50% melting) overlain by pyroxene-type pallasites (30–50% melting), followed by lodranites (5–20% melting) and acapulcoites (<5% melting). Through continuous accretion, this partially differentiated interior becomes capped by undifferentiated chondritic crust, which experiences higher degrees of metamorphism towards the inner layers.

Europe PMC Funders Author Manuscripts

Europe PMC Funders Author Manuscripts

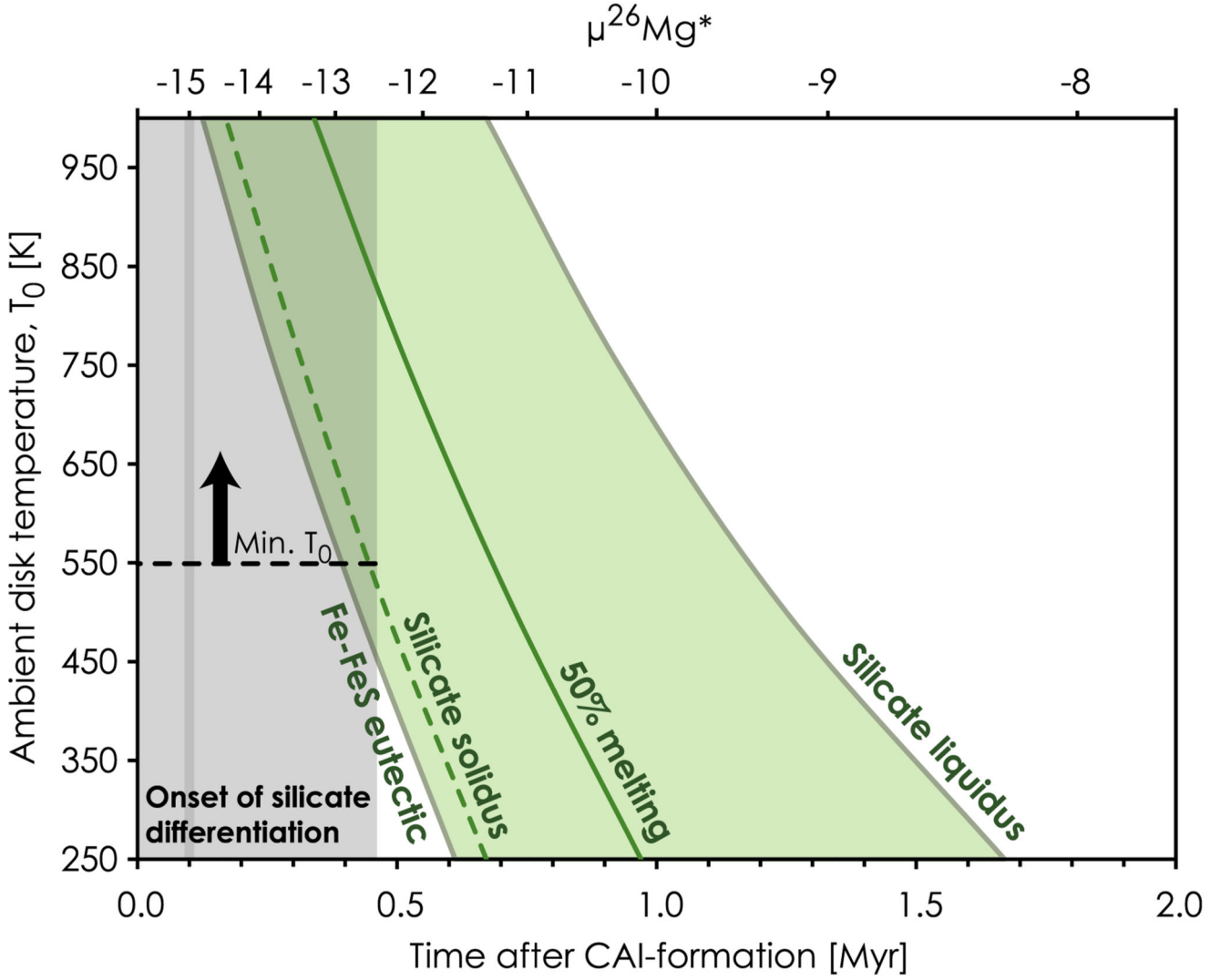

Fig. 8.

Thermal evolution for the heating stage for an ordinary chondrite-type of source rock showing the influence of varying the ambient disk temperature, T_0, on the onset of melting. The subchondritic Al/Mg ratio of the lodranite (Al/Mg = 0.007 and $\mu^{26}Mg^* = -9.7$; Table 3), which experienced 5–20% melting (McCoy et al., 1997), suggests that melt extraction (and thus retarded $^{26}Mg^*$ ingrowth) will occur once the source rock has experienced only a few % melting. In accordance, with models for the temperature evolution of accretion disks (e.g. Ciesla, 2008), the onset of silicate differentiation inferred from the lowest $\mu^{26}Mg^*$ (gray shades) value for Main Group Pallasite olivines is best explained if the planetesimal formed from an initially hot protoplanetary disk at $T_0 > 550$ K.

Europe PMC Funders Author Manuscripts

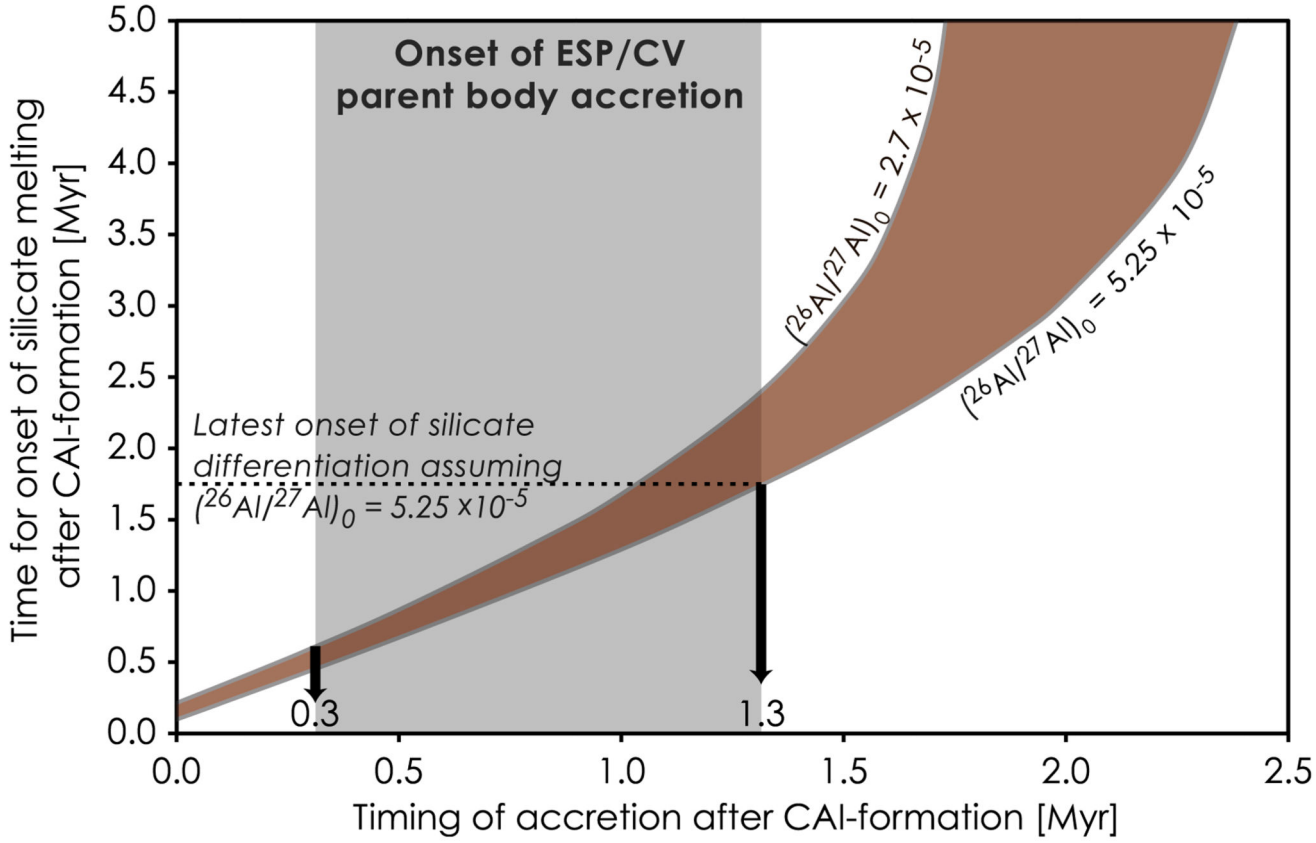

Fig. 9.

Thermal evolution diagram showing the timing for the onset of silicate melting versus accretion time within the centre of a large (100 km in radius) planetesimal of carbonaceous (CV) chondrite-type of composition. The ambient disk temperature was assumed constant at 250 K. The red shaded region marks the plausible time ranges for the onset of melting inferred for an initial $(^{26}Al/^{27}Al)_0$ of 2.7–5.25 × 10^{-5}, where the lower bound is constrained by the proportion of refractory inclusions (with the 'canonical' $(^{26}Al/^{27}Al)_0$) in the CV-type of source rock. $\mu^{26}Mg^*$ evolution in the source rock and the thermal history of the Eagle Station Pallasite (ESP)/CV parent body constrains the onset of its accretion to within 0.3–1.3 Myr post-CAIs (see text for discussion).

Europe PMC Funders Author Manuscripts

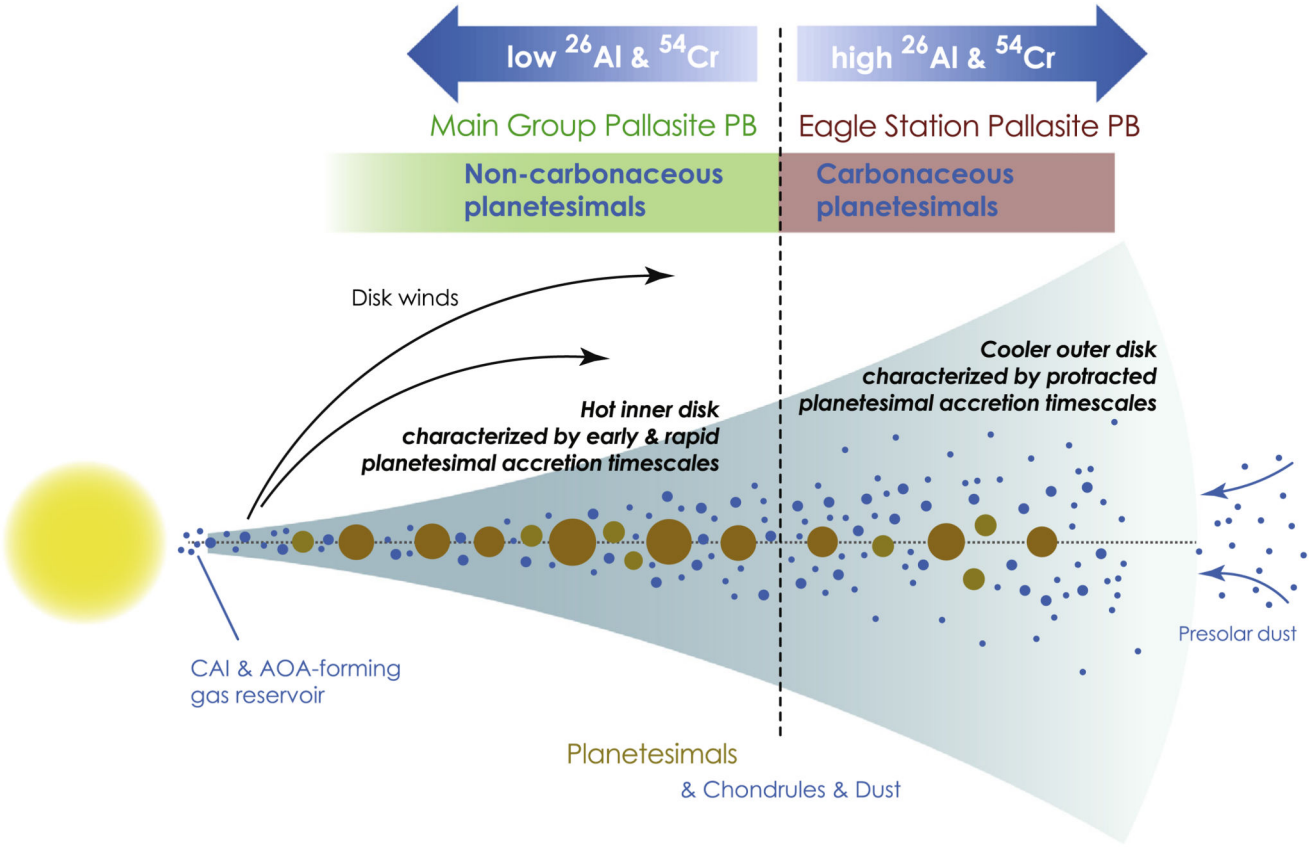

Fig. 10.

Schematic disk model (not to scale) illustrating the proposed planetesimal formation scenario in the solar protoplanetary disk. In the first few 10^5 years after formation of the proto-Sun, the inner disk is hot (>500 K) and characterized by early (<0.25 Myr) and rapid planetesimal formation. These planetesimals (Fig. 7), such as the Main Group Pallasite parent body (**PB**), form from non-carbonaceous disk material characterized by a reduced initial $(^{26}Al/^{27}Al)_0$ of $1–2 \times 10^{-5}$ relative to the 'canonical' value and deficiencies in $\varepsilon^{54}Cr$. Planetesimal formation in the outer disk (Eagle Station/CV parent body) is characterized by prolonged accretion timescales from carbonaceous disk material with initial $(^{26}Al/^{27}Al)_0$ of $>2.7 \times 10^{-5}$ and excesses in $\varepsilon^{54}Cr$.

Europe PMC Funders Author Manuscripts

Table 1

Constants used in the thermal modeling.

Term	Symbol	Value	Units	Note
Thermal conductivity	K	2.1	W m^{-1} K^{-1}	Hevey and Sanders (2006)
Specific heat capacity	C_p	837	J kg^{-1} K^{-1}	Hevey and Sanders (2006)
Density of OC source rock	ρ_{OC}	3800	kg m^{-3}	Lodders and Fegley (1998)
Density of CV source rock	ρ_{CV}	3420	kg m^{-3}	Lodders and Fegley (1998)
Mass fraction of Al in OC source rock		0.0113	–	Hutchison (2004)
Mass fraction of Al in CV source rock		0.0175	–	Hutchison (2004)
Thermal diffusivity of OC source rock	κ_{OC}	6.6×10^{-7}	m^2 s^{-1}	$K/[C_p * \rho]$
Thermal diffusivity of CV source rock	κ_{CV}	7.3×10^{-7}	m^2 s^{-1}	
Ambient disk temperature	T_0	250–1000	K	
^{26}Al decay constant	λ	9.5×10^{-7}	$year^{-1}$	
^{26}Al decay energy		3.12	MeV	Castillo-Rogez et al. (2009)

Table 2

Mg isotope compositions of olivine grains from the Eagle Station and Cold Bay pallasites, as well as carbonaceous chondrites.

Sample	Group[a]	μ^{25}Mg	2se	μ^{26}Mg*	2se	*n*[b]	^{27}Al/^{24}Mg[c]
Cold Bay (USNM633)	PES	−187	6	5.2	1.8	10	<0.0001
Individual Eagle Station olivine grains							
ES-13		−168	4	1.3	1.5	10	<0.0001
ES-3		−197	7	3.1	1.7	10	<0.0001
ES-US (USNM2752)		−163	8	3.3	2.4	10	<0.0001
ES-9		−172	3	4.0	0.9	10	0.00061
ES-GMa		−208	10	4.6	1.6	10	0.00054
ES-8		−180	8	5.0	1.2	10	0.00024
ES-5		−179	25	5.2	0.9	10	0.00035
ES-19		−167	9	5.5	1.0	10	<0.0001
ES-7		−190	7	5.9	2.5	10	0.00044
ES-12b		−188	5	6.0	1.4	10	<0.0001
ES-16		−211	12	6.3	0.7	10	<0.0001
ES-21		−194	5	6.4	1.0	10	<0.0001
ES-2		−175	4	6.5	1.4	10	<0.0001
ES-17		−192	7	6.7	1.3	10	<0.0001
ES-12a		−186	5	8.1	1.8	10	0.00034
ES-18b		−167	19	8.3	2.0	10	<0.0001
ES-6		−184	10	8.9	1.7	10	0.00057
ES-18a		−186	8	9.0	1.6	10	<0.0001
ES-1		−178	6	9.1	1.0	10	<0.0001
ES-GMb		−178	7	9.3	2.4	10	<0.0001
ES-15		−187	9	10.1	0.9	10	0.00014
ES-11		−175	7	12.4	1.1	10	<0.0001
ES-10		−195	7	12.9	2.3	10	0.00027
ES-14		−190	4	14.8	2.0	10	0.00038
Carbonaceous chondrites							
Allende	CV3	−169	8	10.1	3.2	18	0.12890
Murchison	CM2	−159	16	−0.6	3.1	14	0.09680
NWA 4425	CK3	−178	7	7.0	1.8	10	0.11110

[a] PES = Pallasite Eagle Station, CV = carbonaceous chondrite of the Vigarano-type, CM = carbonaceous chondrite of the Murchison-type, CK = carbonaceous chondrite of the Karoonda-type.

[b] Number of measurements.

[c] ^{27}Al/^{24}Mg ratios are accurate to within 2%.

Table 3

Mg isotope compositions of Main Group, pyroxene and ungrouped pallasites, as well as one primitive achondrite.

Sample	Group[a]	μ^{25}Mg	2se	μ^{26}Mg*	2se	*n*[b]	^{27}Al/^{24}Mg[c]
Main group pallasites							
Springwater	PMG	−120	3	−8.2	1.8	10	<0.0001
Philips Co (USNM1695)	PMG	−114	3	−15.0	1.6	10	<0.0001
Dora	PMG	−89	8	−10.1	1.0	10	0.00071
Fukang	PMG	−118	9	−12.6	1.6	10	<0.0001
Brahin	PMG	−83	7	−9.6	1.3	10	0.00004
Brenham	PMG	−116	6	−10.6	1.9	10	<0.0001
Molong	PMG	−113	4	−14.9	2.2	10	<0.0001
Giroux (USNM1574)	PMG	−113	3	−11.1	2.1	10	<0.0001
Krasnojarsk	PMG	−112	12	−9.3	1.7	10	<0.0001
Admire	PMG	−90	12	−10.5	1.5	10	<0.0001
Pyroxene pallasites							
Yamato8451	PxP	−115	10	−14.6	2.3	10	0.00263
Vermillion	PxP	−129	13	−11.6	1.5	10	0.00126
Ungrouped pallasites							
Milton (USNM7816)	Ung.	−97	5	1.6	1.1	10	<0.0001
Zinder	Ung.	−131	9	−11.5	1.6	10	<0.0001
Primitive achondrites							
NWA 4478	Lodranite	−130	6	−9.7	1.4	10	0.00740

[a] PMG = Main Group Pallasite, PxP = Pyroxene Pallasite, Ung. = Ungrouped Pallasite.

[b] Number of measurements.

[c] ^{27}Al/^{24}Mg ratios are accurate to within 2%.